



CCDC DAC-TR-2020-048
July 2020

Whole-Body Postmortem Human Subject (PMHS) Injury Outcome Technical Report

by **Constantine K. Demetropoulos, Kyle A. Ott, David G. Drewry III, Matthew Montoya, John M. Cavanaugh, Jonathan J. Rupp, David R. Barnes, and Kathryn L. Loftis**

DESTRUCTION NOTICE

Destroy by any method that will prevent disclosure of contents or reconstruction of the document.

DISCLAIMER

The findings in this report are not to be construed as an official Department of the Army position unless so specified by other official documentation.

WARNING

Information and data contained in this document are based on the input available at the time of preparation.

TRADE NAMES

The use of trade names in this report does not constitute an official endorsement or approval of the use of such commercial hardware or software. The report may not be cited for purposes of advertisement.



CCDC DAC-TR-2020-048

July 2020

Whole-Body Postmortem Human Subject (PMHS) Injury Outcome Technical Report

**by Constantine K. Demetropoulos, Kyle A. Ott, David G. Drewry III, and
Matthew Montoya**

The Johns Hopkins University Applied Physics Laboratory

John M. Cavanaugh

Wayne State University

Jonathan J. Rupp

University of Michigan Transportation Research Institute

David R. Barnes

SURVICE Engineering Company

Kathryn L. Loftis

CCDC Data & Analysis Center

REPORT DOCUMENTATION PAGE			<i>Form Approved</i> <i>OMB No. 0704-0188</i>		
Public reporting burden for this collection of information is estimated to average 1 hour per response, including the time for reviewing instructions, searching existing data sources, gathering and maintaining the data needed, and completing and reviewing this collection of information. Send comments regarding this burden estimate or any other aspect of this collection of information, including suggestions for reducing this burden to Department of Defense, Washington Headquarters Services, Directorate for Information Operations and Reports (0704-0188), 1215 Jefferson Davis Highway, Suite 1204, Arlington, VA 22202-4302. Respondents should be aware that notwithstanding any other provision of law, no person shall be subject to any penalty for failing to comply with a collection of information if it does not display a currently valid OMB control number. PLEASE DO NOT RETURN YOUR FORM TO THE ABOVE ADDRESS.					
1. REPORT DATE July 2020		2. REPORT TYPE Technical Report		3. DATES COVERED (From - To) 2013 – 2019	
4. TITLE AND SUBTITLE Whole-Body Postmortem Human Subject (PMHS) Injury Outcome Technical Report			5a. CONTRACT NUMBER		
			5b. GRANT NUMBER		
			5c. PROGRAM ELEMENT NUMBER		
6. AUTHOR(S) Constantine K. Demetropoulos, Kyle A. Ott, David G. Drewry III, Matthew Montoya, John M. Cavanaugh, Jonathan J. Rupp, David R. Barnes, and Kathryn L. Loftis			5d. PROJECT NUMBER		
			5e. TASK NUMBER		
			5f. WORK UNIT NUMBER		
7. PERFORMING ORGANIZATION NAME(S) AND ADDRESS(ES) Director U.S. Army CCDC Data & Analysis Center 6896 Mauchly Street Aberdeen Proving Ground, MD			8. PERFORMING ORGANIZATION REPORT NUMBER CCDC DAC-TR-2020-048		
9. SPONSORING / MONITORING AGENCY NAME(S) AND ADDRESS(ES)			10. SPONSOR/MONITOR'S ACRONYM(S)		
			11. SPONSOR/MONITOR'S REPORT NUMBER(S)		
12. DISTRIBUTION / AVAILABILITY STATEMENT DISTRIBUTION STATEMENT A. Approved for public release; distribution is unlimited.					
13. SUPPLEMENTARY NOTES					
14. ABSTRACT The Warrior Injury Assessment Manikin (WIAMan) Program conducted 57 whole-body postmortem human subject (PMHS) tests to characterize biomechanical response under simulated under-body blast. This report details the tests that were conducted and the data collected for each test, as well as an initial analysis of the trends observed across tests. Results discussed include the effects of padding, seat pulse, and pelvis response on pelvis/spine injury; the relationship between floor loads and pulse duration on foot and ankle injuries; and the mechanism of femur fracture.					
15. SUBJECT TERMS Warrior Injury Assessment Manikin, WIAMan, postmortem human subject, PMHS, under-body blast, UBB, injury mechanism, biomechanical response					
16. SECURITY CLASSIFICATION OF:			17. LIMITATION OF ABSTRACT	18. NUMBER OF PAGES	19a. NAME OF RESPONSIBLE PERSON
a. REPORT UNCLASSIFIED	b. ABSTRACT UNCLASSIFIED	c. THIS PAGE UNCLASSIFIED			SAME AS REPORT
					19b. TELEPHONE NUMBER <i>(include area code)</i> (410) 306-0344

Table of Contents

List of Figures	v
List of Tables.....	vi
Executive Summary	vii
1. INTRODUCTION.....	1
1.1 Program Overview	1
1.2 Overview of Whole-Body Experiments	2
2. METHODS.....	5
2.1 Applied Physics Laboratory Test Rig	5
2.1.1 Test Fixture.....	5
2.1.2 Instrumentation Locations and Transducer Types	6
2.1.3 Kinematic Analysis	9
2.1.4 Subject Characteristics	14
2.1.5 Subject Positioning.....	14
2.1.6 Personal Protective Equipment, Boot, and Belt Fitting Procedures.....	15
2.1.7 Data Processing	16
2.2 Wayne State University Test Rig	16
2.2.1 Test Fixture.....	16
2.2.2 Instrumentation Locations and Transducer Types	18
2.2.3 Kinematic Analysis	21
2.2.4 Subject Characteristics	23
2.2.5 Subject Positioning.....	24
2.2.6 Personal Protective Equipment, Boot, and Belt Fitting Procedures.....	25
2.2.7 Data Processing	26
2.3 University of Michigan Transportation Research Institute Test Rig	26
2.3.1 Test Fixture.....	26
2.3.2 Instrumentation Locations and Transducer Types	27
2.3.3 Kinematic Analysis	32
2.3.4 Subject Characteristics	35
2.3.5 Subject Positioning.....	35
2.3.6 Personal Protective Equipment, Boot, and Belt Fitting Procedures.....	36
2.3.7 Data Processing	36
3. RESULTS.....	38
3.1 Effects of Padding, Seat Pulse, and Pelvis Response on Pelvis/Spine Injury.....	42
3.2 Relationship between Floor Loads and Pulse Duration on Foot and Ankle Injuries	49
3.3 Mechanism of Femur Fracture	51
4. DISCUSSION AND CONCLUSIONS.....	57
5. REFERENCES AND DOCUMENTS	59
Appendix A – List of Acronyms.....	A-1

Table of Contents

Appendix B – Glossary	B-1
Appendix C – Classification of Injuries.....	C-1
Appendix D – Distribution List	D-1

List of Figures

Figure 1.	Seat cushions utilized in the whole-body experiments	4
Figure 2.	Rendering of the VALTS in front and isometric views	6
Figure 3.	Rig instrumentation locations	7
Figure 4.	Subject instrumentation locations	9
Figure 5.	Target posture.....	15
Figure 6.	WSU horizontal sled system with the occupant positioned on the seat with a 5-point belt	17
Figure 7.	The two large-capacity snubbers mounted to the barrier are used to decelerate the sled deck, while the pre-crushed aluminum honeycomb blocks attached to the barrier are used to decelerate the seat fixture and produce a target TTP for the seat	18
Figure 8.	Rig instrumentation locations	19
Figure 9.	Subject instrumentation locations	21
Figure 10.	Target position	25
Figure 11.	UMTRI test rig.....	27
Figure 12.	Rig instrumentation locations	28
Figure 13.	Subject instrumentation locations	31
Figure 14.	Target position	36
Figure 15.	Peak seat Fz and sacrum velocity and TTP.....	38
Figure 16.	Effects of peak seat loads on pelvic ring injuries.....	42
Figure 17.	Effects of peak sacrum velocity on pelvic ring injuries	43
Figure 18.	Effects of peak seat loads on sacrum injuries	44
Figure 19.	Effects of peak sacrum velocity on sacrum injuries.....	44
Figure 20.	Effects of peak seat loads on AIS2+ lumbar spine injuries	45
Figure 21.	Effects of peak sacrum velocity on AIS2+ lumbar spine injuries.....	46
Figure 22.	Effects of peak seat loads on AIS3+ lumbar spine injuries	46
Figure 23.	Effects of peak sacrum velocity on AIS3+ lumbar spine injuries.....	47
Figure 24.	Effects of peak seat loads on AIS2+ thoracic spine injuries.....	48
Figure 25.	Effects of peak sacrum velocity on AIS2+ thoracic spine injuries	48
Figure 26.	Effects of peak foot force and duration on lower extremity injuries	49
Figure 27.	Effects of peak heel force and duration on lower extremity injuries	50
Figure 28.	Effects of total foot impulse and duration on lower extremity injuries	51
Figure 29.	Initial positioning WH04-002 (left) and WS10-001 (right).....	52
Figure 30.	Femoral fractures of WH04-002 (top) and WS10-001 (bottom)	53
Figure 31.	Vertical femoral acceleration of WH04-002 (left) and WS10-001 (right)	53
Figure 32.	Seat force response for WS10-001; note the spikes in the signal are indicative of cable yank	54
Figure 33.	Seat force response for WS10-002.....	55
Figure 34.	Kinematic displacement of WH04-001 and WH04-002 (top) and time-series images for WH04-002 (bottom).....	56
Figure 35.	Total injuries from WIAMan whole-body experiments.....	57

List of Tables

Table 1.	Whole-Body Conditions Tested.....	3
Table 2.	Masses and Instrumentation Used for Mass Compensation	7
Table 3.	Subject Instrumentation Locations.....	8
Table 4.	Rigidly Installed Kinematic Marker Locations.....	10
Table 5.	Kinematic Surface Marker Locations	11
Table 6.	Rig Kinematic Marker Locations.....	12
Table 7.	Calculated Kinematic Descriptions.....	13
Table 8.	Subject Acceptance Criteria.....	14
Table 9.	Masses and Instrumentation Used for Mass Compensation	19
Table 10.	Subject Instrumentation Locations.....	20
Table 11.	Surface Marker Anatomical Locations	22
Table 12.	Surface Marker Boot Locations	22
Table 13.	Rig Kinematic Marker Locations.....	23
Table 14.	Calculated Kinematic Descriptions.....	23
Table 15.	Subject Acceptance Criteria.....	24
Table 16.	Masses and Instrumentation Used for Mass Compensation	28
Table 17.	Subject Instrumentation Locations.....	30
Table 18.	Rigidly Installed Kinematic Marker Locations.....	32
Table 19.	Kinematic Surface Marker Locations	33
Table 20.	Rig Kinematic Marker Locations.....	34
Table 21.	Calculated Kinematic Descriptions.....	34
Table 22.	Subject Acceptance Criteria.....	35
Table 23.	APL Injury Summary Table.....	39
Table 24.	WSU Injury Summary Table	40
Table 25.	UMTRI Injury Summary Table	41
Table 26.	WH04-002 and WS10-001 Specimen Information.....	51
Table 27.	WH04-002 and WS10-001 Test Conditions	52
Table C.1.	APL Injury Summary.....	C-2
Table C.2.	WSU Injury Summary	C-6
Table C.3.	UMTRI Injury Summary	C-8

Executive Summary

A total of 57 whole-body postmortem human subject (PMHS) tests that were conducted to characterize biomechanical response under simulated under-body blast (UBB) and evaluate injury outcomes are summarized in this report. The test conditions selected for these experiments were chosen to characterize PMHS responses and injury thresholds under high-rate vertical loading to support the development of the Warrior Injury Assessment Manikin (WIAMan). These conditions include tests under noninjurious input conditions to assess biomechanical response and injurious conditions to produce injuries that could be utilized to evaluate the injury prediction capabilities of the WIAMan. Theater-relevant injuries were targeted to include pelvic ring, lumbar spine, and foot–ankle complex fractures.

The floor and seat velocity profiles used in these tests were selected to represent UBB loading conditions that occur across the range of specifications established for the WIAMan program, where minimal PMHS data existed previously. Injury outcomes were sought from noninjurious up through an injury severity that would be within the range of mitigation efforts. Key measurements made in these tests included floor and seat accelerations, forces applied to the foot and pelvis, accelerations and angular velocities measured at discrete locations on PMHS components, and strain gauges and acoustic emission measurements to identify fracture timing.

Results of these tests met the goal of providing biomechanical data from noninjurious levels through reasonable severity to span the intended use case of the WIAMan. This report details the tests that were conducted and the data collected for each test, as well as an initial analysis of the trends observed across tests. An independent U.S. Army effort is currently underway to use data from these whole-body experiments to aid in the validation of WIAMan injury assessment curves.

1. INTRODUCTION

1.1 Program Overview

The Warrior Injury Assessment Manikin (WIAMan) program is an Army-sponsored initiative to develop an advanced anthropomorphic test device (ATD) that can be utilized to predict injuries for seated vehicle occupants in under-body blast (UBB) and other military-relevant vertical loading environments. As part of this program, the first comprehensive set of biomechanical response and injury tolerance data has been collected under high-rate vertical loading representative of that experienced by seated vehicle occupants in UBB.

Biomechanical response and tolerance data have been collected from tests of whole-body postmortem human subjects (PMHSs) and PMHS components. The first set of whole-body PMHS tests served to characterize biomechanical response for the purpose of developing biofidelity response corridors (BRCs). These tests were conducted at lower severity input conditions, as the goal was not to produce injury, but rather establish specifications for human kinematics and the interactions between humans and the seat environment to act as performance targets for the WIAMan Gen1 test device.

Human injury probability curves (HIPCs), which are probabilistic dose-response relationships that relate the magnitude of a mechanical quantity to the risk of injury (typically fracture), were developed from component PMHS tests. Match-paired tests of ATD and PMHS components were performed to relate human injuries to WIAMan Gen1 component responses. Match-paired tests were performed with the full WIAMan Gen1 using the whole-body PMHS test BRC input conditions primarily to evaluate biofidelity. A secondary use of these tests was to evaluate the injury assessment reference curves (IARCs) developed from match-paired component tests. However, BRC whole-body PMHS tests were conducted at lower severity conditions such that it was not possible to utilize the BRC whole-body PMHS test results to assess the WIAMan IARCs over the full range of UBB-relevant conditions that were defined by experiments conducted by the U.S. Army. To address the need for additional tests conducted at more severe UBB-relevant conditions, a second set of whole-body PMHS tests were conducted to generate whole-body response data under injurious loading conditions.

Together with these two types of tests, a third type, termed ancillary, was also conducted. Ancillary tests were intended for a full series of experiments. However, initial results suggested that a full series of experiments was not required. Some ancillary tests were BRC experiments that were intended to be subinjurious, but produced injuries. Data from all three types of experimental conditions are included in this report and summarize the observed injuries from whole-body experiments conducted across three performers of the WIAMan program. The level of detail in the current report enables future users to understand methods and key injury findings

related to existing PMHS whole-body test injury outcomes conducted under the WIAMan program.

1.2 Overview of Whole-Body Experiments

Whole-body experimental conditions were selected to span a range of UBB-relevant conditions as defined by the U.S. Army. These conditions are summarized in Table 1 and are grouped into three categories of tests, indicated by the naming convention. Tests that begin with “WH” were designed to produce BRC-relevant conditions with limited injuries. Tests that begin with “WS” were severe test conditions intended to produce injuries. Tests that begin with “WA” were ancillary tests that were run with the intent to serve as “WH” or “WS” conditions, but were not selected for a complete test series.

Table 1. Whole-Body Conditions Tested

Test Condition	Seat Velocity	Seat TTP	Floor Velocity	Floor TTP	Posture*	Seat Type*	PPE*	Tests at APL**	Tests at WSU**	Tests at UMTRI**
WH01	4	5	4	5	90-90-90	Rigid	None	3	1	1
WH02	4	5	4	5	90-90-90	Rigid	Medium			4
WH03	4	10	6	5	90-90-90	Rigid	None	3	2	
WH04	4	10	6	5	90-90-90	Rigid	Medium	3	3	
WH06	4	55	8	2	90-90-90	Rigid	Medium		3	
WH07	4	40	7	2.75	Acute	Rigid	Medium			3
WH08	4	30	8	2	Obtuse	Rigid	Medium	3		
WH11	5	10	7.5	2.5	90-90-90	V10 Cushion	Medium			3
WH12	3	8	8	2	OEM	OEM Seat	Medium	3		
WS01	6	5	8.5	2.5	90-90-90	Ethafoam Cushion	Medium			2
WS04	6	20	8.5	2.5	90-90-90	Ethafoam Cushion	Medium	1		
WS09	12	5.5	16.5	2	90-90-90	Ethafoam Cushion	Medium		1	
WS10	10	7.5	15.5	2.5	90-90-90	V10 Cushion	Medium	3		
WS11	9	5	13	2.5	90-90-90	V10 Cushion	Medium		3	
WS12	6.5	7.5	10	2.5	90-90-90	Rigid	Medium			3
WA01	3	5	3	5	90-90-90	Rigid	None	1		
WA02	6	10	8	5	90-90-90	Rigid	Medium			1
WA03	6	5	6	5	90-90-90	Rigid	None		1	
WA04	6	10	8	5	90-90-90	Rigid	None	1		
WA05	6	10	8	5	90-90-90	Ethafoam Cushion	None			1
WA06	6	10	8	5	90-90-90	Ethafoam Cushion	None	1		
WA07	6	10	8	5	90-90-90	V1 Cushion	Medium	1		
WA08	6	10	8	5	90-90-90	V1 Cushion	None			1
WA09	5	10	8	2.5	90-90-90	V10 Cushion	Medium			1

* Posture, seat types, and personal protective equipment (PPE) are defined in the following text.

** Bold numbers indicate conditions with match-paired WIAMan Gen1 data (all except WS09).

Seat cushions referenced in Table 1 included a rigid seat or a rigid seat covered by one of three seat cushions, as shown in Figure 1. The materials included 2-inch nominal thickness Ethafoam 4101FR (Sealed Air Corporation, Charlotte, NC), ½-inch-thick Poron XRDMA 12500, and ½-inch-thick Poron XRDMA 09500 (Rogers Corporation, Chandler, AZ) in various configurations as shown.



Figure 1. Seat cushions utilized in the whole-body experiments

All specimens were outfitted with Belleville 390 DES men’s hot weather desert tan combat boots (Belleville Boot Company, Belleville, IL) and tests with a specified value in the PPE column of Table 1 indicate the use of medium PPE. The medium PPE used is described in the individual methods section for each performer. The postures tested in these experiments include 90-90-90, acute, and obtuse. The 90-90-90 posture serves as a baseline, where the joint angles at the hip, knee, and ankle were set to 90°. The acute posture places the subject in a forward slouched position with the heels drawn toward the seat. The obtuse posture places the subject in a reclined position with the legs extended forward. These are described in the referenced positioning document (Rupp & Reed, 2015) and in the corresponding methods sections.

2. METHODS

2.1 Applied Physics Laboratory Test Rig

2.1.1 Test Fixture

The Johns Hopkins University Applied Physics Laboratory (APL) test device, the Vertically Accelerated Load Transfer System (VALTS), is a vertical sled system designed to generate a range of high-velocity, short-duration input pulses. Standing at a total height of 10.5 m, the VALTS has the capacity to simultaneously vertically accelerate two seated surrogates that may be ATDs, PMHSs, or both (Figure 2). The VALTS has one 1.27- × 1.52-m primary platform to which a seat system is mounted, and two secondary 0.36- × 0.59-m platforms located in front of the primary platform that serve as the right and left occupant floor plates. Both floor plates are independently programmed and driven from each other, and are also actuated independently from the primary platform. The total achievable travel of the primary platform is 3.1 m, while the floor platforms are constrained between displacement limits that restrict their travel to 0.05 m. The VALTS achieves high impact energies through pneumatic propulsion of precision-guided ballistic masses into both the primary and secondary platforms. These ballistic masses are propelled by a single 25.4-cm-diameter, high-pressure nitrogen actuator for the primary platform and two independent 10.2-cm-diameter nitrogen actuators for each of the secondary platforms. Elastomers with a linear response are placed between the ballistic mass and the platform bases to produce the desired pulse duration, while the pneumatic pressure system controls the impact velocity. Input velocities on the VALTS ranged from 2 to 10 m/s with durations from 2 to 35 ms for the primary (seat) platform and from 2 to 16.5 m/s with durations from 1 to 10 ms for the secondary (floor) platforms. Additionally, isolation of the different test platforms allows for independent timing of the applied loads, which supports the study of differential timing between the floor and seat. Pneumatic brakes are incorporated within the VALTS linear bearing system to both control the descent of the primary platform and prevent slam-down after a test. For this study, only the initial accelerative period of loading was investigated with simultaneous floor and seat loading pulses.

Seat cushions were utilized as described in Table 1. When a seat cushion was present, the surface of the cushion was covered with a layer of gaffer's tape. Otherwise, the PMHS was placed directly upon the rigid surface of the seat.

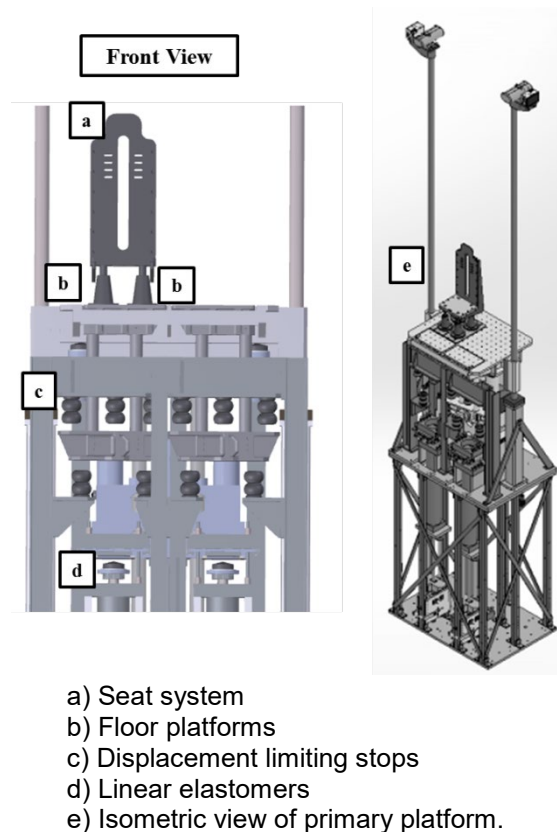


Figure 2. Rendering of the VALTS in front and isometric views

2.1.2 Instrumentation Locations and Transducer Types

The test fixture incorporated an array of uniaxial load cells and accelerometers at the occupant–seat and occupant–footplate interfaces (Figure 3 and Table 2). The seat load cell configuration included uniaxial load cells at the sacrum, left and right ischium, and left and right thigh, allowing for the analysis of seat load distribution between the component seat plates (Rupp et al., 2016), as well as the ability to sum the individual loads to calculate a total seat force. Footplate load cells measured the forefoot and heel forces that could be used to calculate total floor force. Associated accelerometers measured footplate acceleration and were used for mass correction of loads. Fixture velocities were calculated by integrating acceleration signals at the floor and seat.

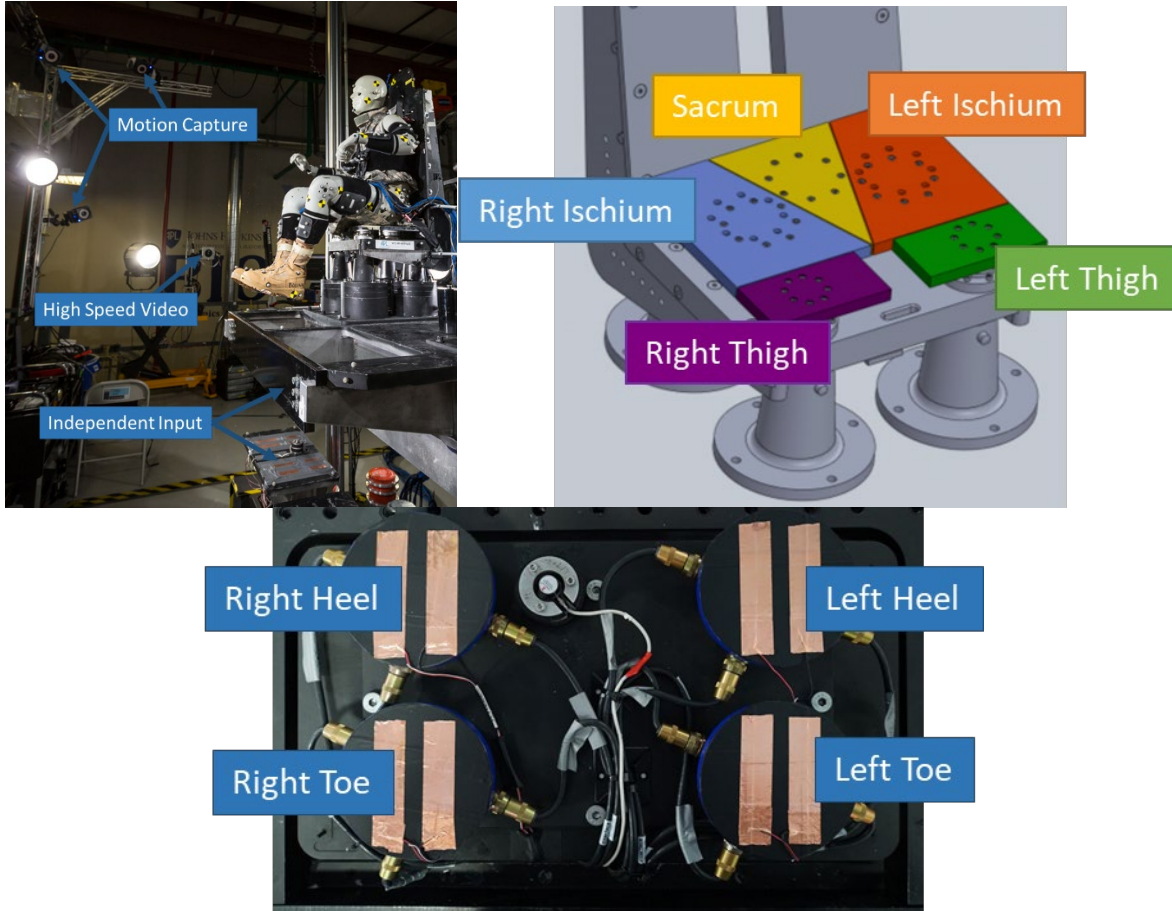


Figure 3. Rig instrumentation locations

Table 2. Masses and Instrumentation Used for Mass Compensation

Location	Plate Mass (kg)	Load Cell Names	Load Cell Model	Accelerometer Name	Accelerometer Model
Left heel	0.6	L Heel FOR	5210XYZ	Floor ACC	Endevco_72701A-20k
Right heel	0.6	R Heel FOR	5210XYZ	Floor ACC	Endevco_72701A-20k
Left forefoot	0.6	L Toe FOR	5210XYZ	Floor ACC	Endevco_7264D-2000
Right forefoot	0.6	R Toe FOR	5210XYZ	Floor ACC	Endevco_7264D-2000
Sacrum	2.2	Sacrum FOR	LWPF1-50kN	Sacrum ACC	Endevco_7270A-6k
Left IT	3.3	L Ischium FOR	LWPF1-50kN	L Ischium ACC	Endevco_7270A-6k
Right IT	3.3	R Ischium FOR	LWPF1-50kN	R Ischium ACC	Endevco_7270A-6k
Left thigh	1.3	L Thigh FOR	LWPF1-20kN	L Thigh ACC	Endevco_7270A-6k
Right thigh	1.3	R Thigh FOR	LWPF1-20kN	R Thigh ACC	Endevco_7270A-6k

Notes: ACC = acceleration, FOR = force, IT = ischial tuberosity

The PMHS instrumentation included six-degree-of-freedom (6DOF) sensors (6DX, Diversified Technical Systems, Inc.), uniaxial accelerometers (7264 and 7270A, Endevco), acoustic emission sensors (Nano 30, Physical Acoustics), and strain gauges (KFW-2-350-D17-11,

Kyowa). The types and locations of these sensors and the orientations of strain gauges are provided in Table 3 and Figure 4. The 6DX sensors measured X-, Y-, and Z-accelerations (A_x , A_y , and A_z , respectively) and X-, Y-, and Z-angular rates (AR_x , AR_y , and AR_z , respectively). The 6DX sensors were rigidly mounted to the skull (3 cm superior to the Frankfort Plane at the level of the tragion) using screws with Helicoil thread inserts, thoracic vertebrae (T1, T5, T8, T12, and L3), sacrum (S1–S3 level), superior pubic rami, distal femurs, and proximal tibias. Screws were placed in the bone for mounting these subjects, with the exception of the pubic ramus in which hose clamps were used to mount the sensors. The distal femur 6DX sensors were located proximal to the distal femur at a distance of 25% of the total femur length. The proximal tibia 6DX sensors were located distal to the most proximal portion of the bone at a distance of 25% of the total tibia length. Two 7270A accelerometers were installed on the medial surface of the left and right calcaneus, respectively, and oriented parallel to the leg long axis to measure A_z . Modified 7264 accelerometers with one flange removed were installed on the cervical vertebral bodies of C2 and C4 just lateral of the mid-sagittal plane in the superior-inferior direction. A computed tomography (CT) scan was conducted after the instrumentation was installed, but prior to testing, to document the sensor positions relative to the skeleton.

Table 3. Subject Instrumentation Locations

6DX	Strain Gage*	Acoustic Emission Sensor	7264/7270A Uniaxial Accelerometer
Head	Left Rib 10	T6	C2
Sternum	Right Rib 10	T8	C4
Left Superior Pubic Ramus	Left ASIS	T10	Left Calcaneus
Right Superior Pubic Ramus	Right ASIS	L1	Right Calcaneus
Left Distal Femur	Left Superior Pubic Ramus	L3	
Right Distal Femur	Right Superior Pubic Ramus	L4	
Left Proximal Tibia	Left Proximal Femur	Left Iliac Wing	
Right Proximal Tibia	Right Proximal Femur	Right Iliac Wing	
T1	Left Distal Femur	Left Tibia	
T5	Right Distal Femur	Right Tibia	
T8	Left Proximal Tibia	Left Calcaneus	
T12	Right Proximal Tibia	Right Calcaneus	
L3	Left Distal Tibia		
Sacrum (S1–S3)	Right Distal Tibia		
	Left Calcaneus		
	Right Calcaneus		

* Strain gauges were placed along the long axes of long bones, the circumferential direction of ribs, along the direction of the pelvic ring for the pubic ramus, along the direction of the iliac crest for the anterior superior iliac spine (ASIS), and fore to aft for the calcaneus locations.

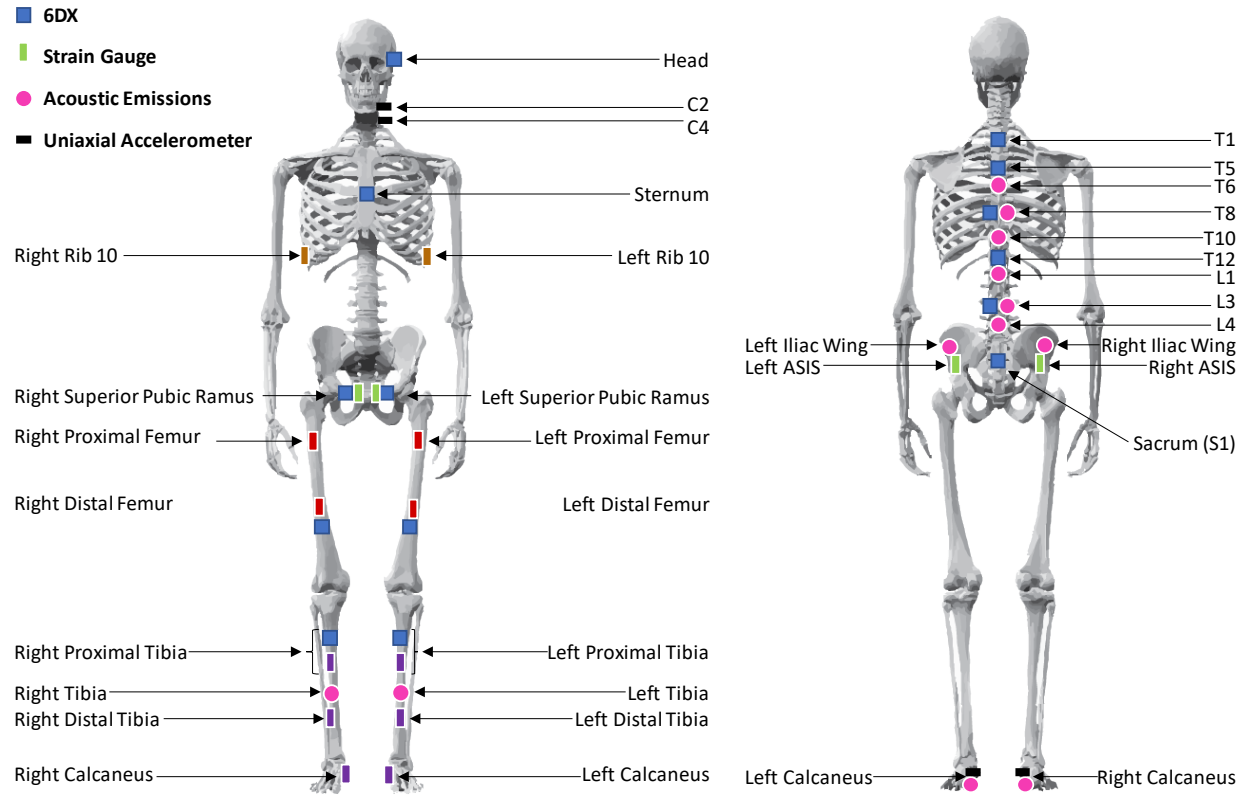
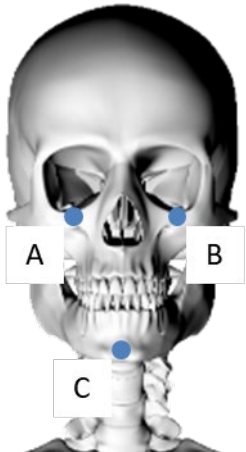
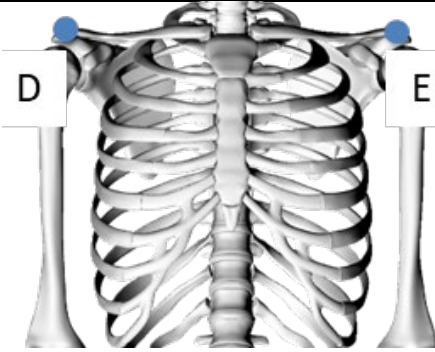
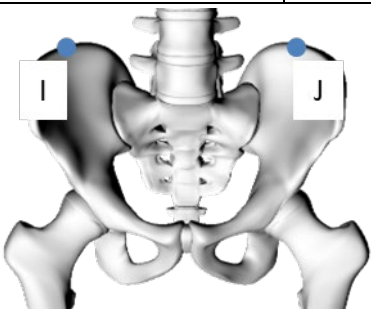
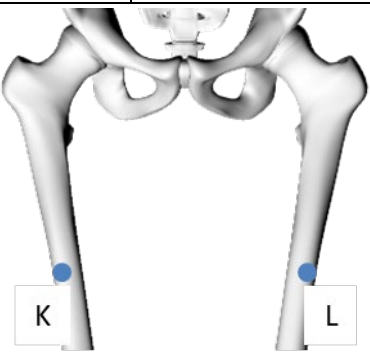


Figure 4. Subject instrumentation locations

2.1.3 Kinematic Analysis

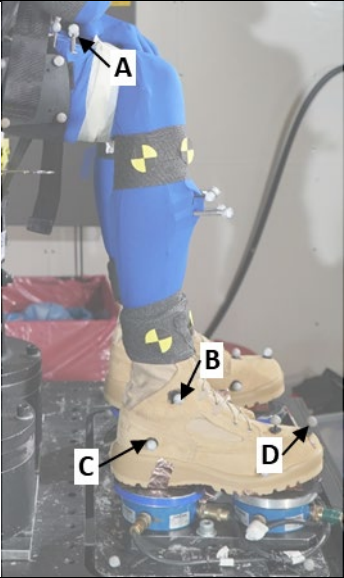
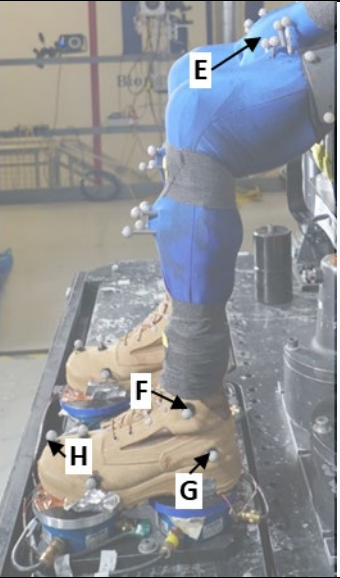
Spherical markers (rigidly attached to bone, either through screw fixation or the use of cyanoacrylate glue) or quadrant marker decals (adhered to the surface of clothing or PPE) were placed at various skeletal and surface landmarks for kinematic tracking. Tracked locations included the following: head (three spherical markers at various locations of the face) (Table 4), shoulders (spherical markers at left and right acromion), pelvis (subject-specific clamps attached to the posterior superior iliac spine [PSIS] bilaterally), femur (quadrant markers proximal and distal, and spherical markers), knee (motion transformed to this location using coordinate measurement data), proximal tibia (quadrant markers attached to 6DX sensor mount and spherical markers), and boots (left and right forefoot, left and right hindfoot, left and right lateral malleolus) (Tables 4 and 5). Knee motion was tracked using coordinate measurement data from femur motion (Table 5). Various points on the fixture were tracked to define and translate the coordinate system as the test fixture moved through the tracking frame (Table 6). Motion tracking and calibration were performed using motion analysis software (VICON).

Table 4. Rigidly Installed Kinematic Marker Locations

		
<p>A) Head_Anterior_Lateral_Right B) Head_Anterior_Medial_Left C) Head_Anterior_Medial</p>	<p>D) Shoulder_Right_Lateral E) Shoulder_Left_Lateral</p>	<p>G) Femur_Right_Anterior* H) Femur_Left_Anterior*</p>
		
<p>I) Pelvis_Right_P SIS J) Pelvis_Left_P SIS</p>	<p>K) RThigh_Prox_Femur L) LThigh_Prox_Femur</p>	

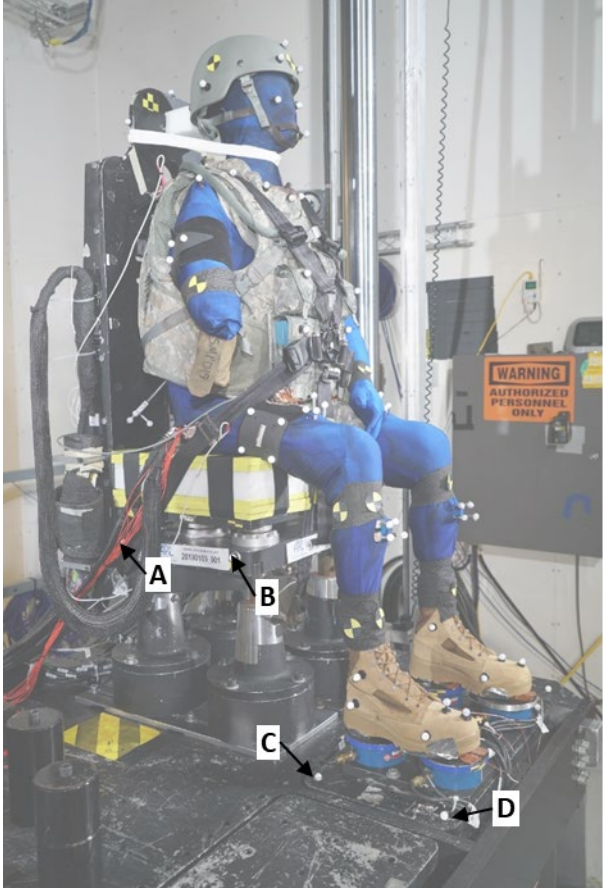
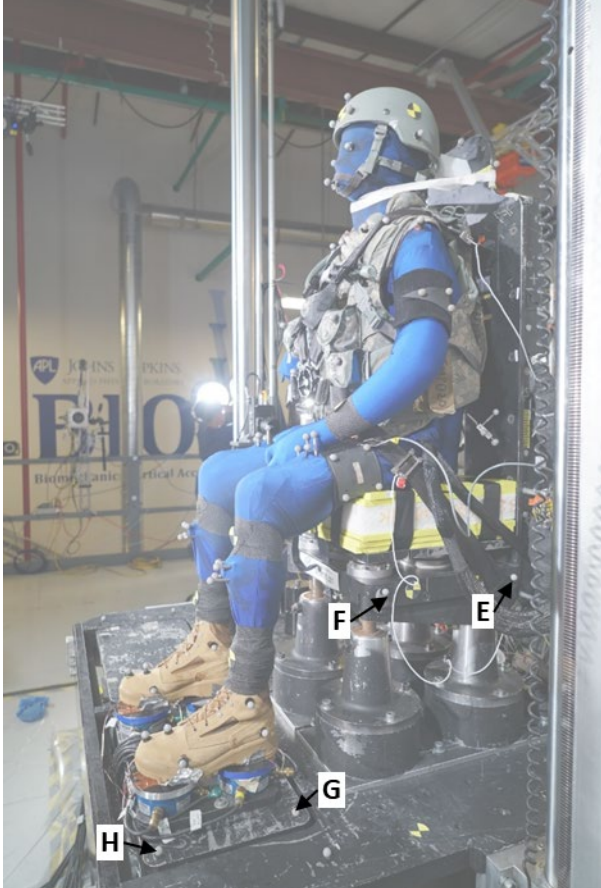
*Measured points transformed to knee using collected coordinate measurement device points.

Table 5. Kinematic Surface Marker Locations

 <p>A photograph of a person's right leg in a blue motion capture suit and a tan boot, standing on a platform. Four white surface markers are visible: A on the knee, B on the lateral superior part of the boot, C on the lateral posterior part of the boot, and D on the lateral anterior part of the boot. Arrows point from the labels to the markers.</p>	 <p>A photograph of a person's left leg in a blue motion capture suit and a tan boot, standing on a platform. Four white surface markers are visible: E on the knee, F on the lateral superior part of the boot, G on the lateral posterior part of the boot, and H on the lateral anterior part of the boot. Arrows point from the labels to the markers.</p>
<p>A) Knee_Right_Lateral* B) Boot_Right_Lateral_Superior C) Boot_Right_Lateral_Posterior D) Boot_Right_Lateral_Anterior</p>	<p>E) Knee_Left_Lateral* F) Boot_Left_Lateral_Superior G) Boot_Left_Lateral_Posterior H) Boot_Left_Lateral_Anterior</p>

* Knee motion transformed using coordinate measurement data from femur motion.

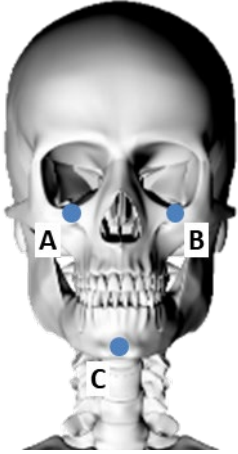
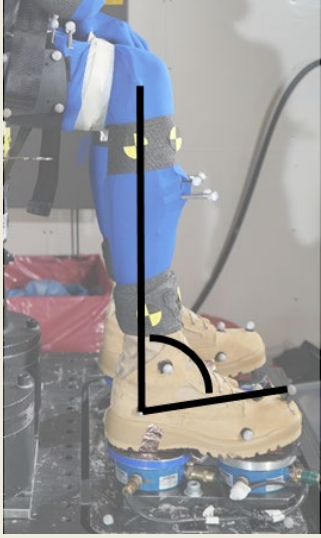
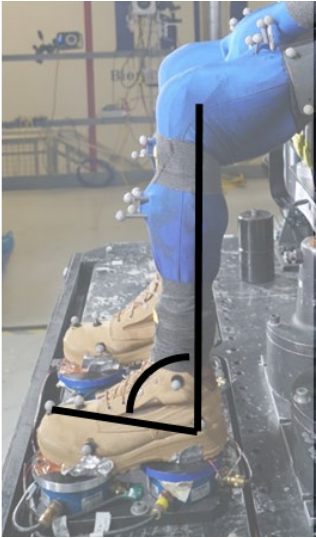
Table 6. Rig Kinematic Marker Locations

	
<p>A) Seatpan_Right_Aft*</p> <p>B) Seatpan_Right_Fore</p> <p>C) Rig_Right_Aft</p> <p>E) Floor_Right_Fore</p>	<p>E) Seatpan_Left_Aft</p> <p>F) Seatpan_Left_Fore</p> <p>G) Floor_Left_Aft</p> <p>H) Floor_Left_Fore</p>

*Exact locations of seatpan aft and floor fore may vary between tests based on visibility from camera views.

The location of the head center of gravity (CG) was calculated at each point in time using the skeletal surface markers shown in Table 7 based on the head CG location relative to these markers calculated using CT data with the procedure defined in the W0084 technical guidance document (Bass et al., 2016). In this calculation, it was assumed that the head CG does not change during the event. Foot angle was also calculated using the landmarks listed in Table 7.

Table 7. Calculated Kinematic Descriptions

Location	Description	Image
Head_Center	Calculated position using a rigid-body transformation from rigidly installed kinematic markers on head (Table 4) and head CG calculated from CT scan	
Boot_Knee_Right	Included foot angle between Knee_Right_Lateral to Boot_Right_Lateral_Superior and Boot_Right_Lateral_Posterior to Boot_Right_Lateral_Anterior	
Boot_Knee_Left	Included foot angle between Knee_Left_Lateral to Boot_Left_Lateral_Superior and Boot_Left_Lateral_Posterior to Boot_Left_Lateral_Anterior	

2.1.4 Subject Characteristics

Table 8 provides the acceptance criteria for subjects tested by APL for all PMHS experiments. All subjects were within predefined acceptable ranges, or received an exception from the sponsor. Standard subject anthropometry measured in accordance with reference document W0080, Minimum Pre-Test Anthropometry Requirements for Scaling (Bass et al., 2013).

Table 8. Subject Acceptance Criteria

Test Series ID	Age (yrs)	Gender	Height (cm)	Weight (kg)	BMI	T-Score (L1–L4)
Acceptance Criteria	18	M	165	64	18	-1.0
	-		-	-	-	-
	80		186	106	35	+2.5

2.1.5 Subject Positioning

Subject positioning was based on the relative locations of skeletal surface landmarks, together with seated X-ray images. Figure 5 shows the target postures and highlights important joint angles and relative positions of landmarks for the example of a 90-90-90 posture. (Other postures utilized the same method with guidance from documented positioning methods [Rupp & Reed, 2015].) Landmarks were identified through palpation. Landmarks on the pelvis were determined through a lateral X-ray while seated on the test rig. Pelvis angle was defined as the angle of the line formed by the midpoint between the left and right ASISs (mid-ASIS) and the pubic symphysis landmark compared in reference to vertical.

A three-dimensional (3-D) coordinate measurement device (Romer Absolute Arm, Cobham, Great Britain) was used to measure the position of the PMHS prior to each test. During the positioning process, 3-D locations were recorded at various landmarks and checked against target relative orientations. When measurements fell outside of tolerance, the PMHS was adjusted accordingly and remeasured until within tolerance or as close to the target range as the PMHS anatomy permitted. Tape was used to secure each PMHS head in the proper posture by running a strip or multiple strips of tape from the PMHS head and/or helmet to a rigid location on the test fixture. Tape mounting locations varied with each test, but tape was typically affixed to the PMHS chin, nose, and helmet (see Figure 5 for an example). For each PMHS, the minimum number of strips of tape that were sufficient to secure the head in the proper posture were used. Tape was pre-cut approximately 90% across its width immediately prior to each test such that the tape severed upon initiation of the loading event. In all tests, all strips of tape were completely severed at the beginning of the loading event; PMHS head motion did not appear to be influenced by tape placement. Final coordinates were documented immediately before each test.

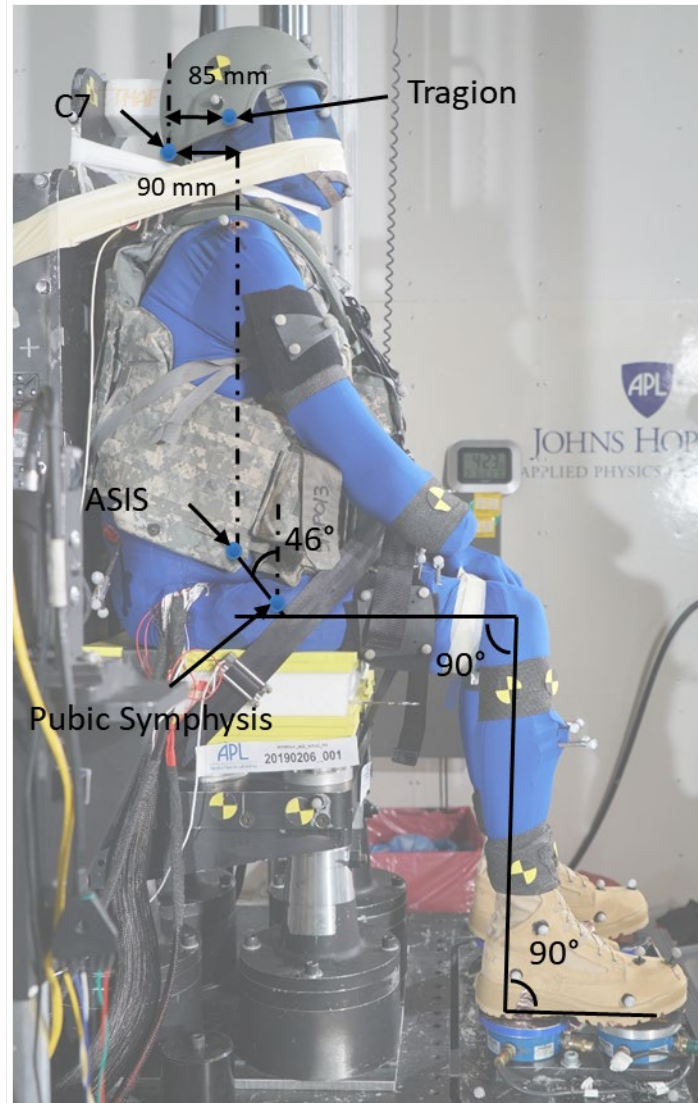


Figure 5. Target posture

Target postures were based on the postures assumed by midsize male Soldiers seated in a military vehicle seat with a vertical back and horizontal seat cushion based on Reed and Ebert (2013). Positioning was performed following the procedure described by Rupp and Reed (2015). When positioning subjects, the highest priority was given to matching pelvis angle, head position and angle, and foot and knee angles. Lower priority was given to acromion position, as some subjects were missing forearms, preventing the use of the arm to control shoulder position.

2.1.6 Personal Protective Equipment, Boot, and Belt Fitting Procedures

PPE, including advanced combat helmet (ACH), improved outer tactical vest (IOTV), and Belleville 390 DES men's hot weather desert tan combat boots (Belleville Boot Company, Belleville, IL), were fitted to the PMHS in accordance with reference documents W0058 (Helmet Fitting Procedures [WIAMan Biomechanics Team, 2013a]), W0059 (IOTV Fitting

Procedures [WIAMan Biomechanics Team, 2013b]), and W0060 (Boot Fitting Procedures [WIAMan Biomechanics Team, 2013c]), respectively. The routing and fitting of the 5-point seatbelt restraint harness was performed in accordance with reference document W0070 (Belt Fitting Procedures [WIAMan Biomechanics Team, 2013d]).

2.1.7 Data Processing

All signals were processed following the procedures used for BRC development. Accelerometers and seat/floor load cell data were filtered using a low-pass 4th-order digital phaseless Butterworth filter with a cutoff frequency of 3 kHz. Angular rate data were filtered using a cutoff frequency of 1650 Hz. DTS 6DX transducer measurements were transformed to standardized locations relative to skeletal anatomic landmarks using the procedure developed by the Signal Conversion Tiger Team (SCoTT) reported by Slykhouse et al. (2019). Seat and floor velocities were calculated by integrating Z-axis accelerometers located under the center of the seat and under the center of the left and right feet.

Time to peak (TTP) velocities for the floor and seat were calculated using the method defined by Spink (2014). This method involves a baseline shift and integration of the acceleration time history, the peak (largest negative) velocity within a time frame of interest, and identification of all local minima less than 90% of the absolute peak. The local minimum just prior to the absolute peak is selected as the new peak velocity and points corresponding to 5%, 20%, and 95% of the final peak velocity are determined. If the velocity history exhibits a monotonic fall between 5% and 20%, the velocity slope is calculated between the points at 5% and 95% of the peak velocity. If the velocity history is not monotonic between 5% and 20%, the data point immediately following the last positive derivative in the window is identified and used to replace zero as the baseline for the 5% calculation. The start and end times are determined by calculating the times at which the equation defining the velocity slope are equal to zero and peak velocity, respectively. The TTP is the difference between the calculated ending and starting times.

2.2 Wayne State University Test Rig

2.2.1 Test Fixture

The Wayne State University (WSU) test fixture is an aluminum, horizontal, decelerative system comprising a sled deck (WHAM IV), a rigid seat on rails, and a movable footplate (Figure 6). Two rails are mounted to the sled deck, parallel to the long axis of the sled. A rigid seat fixture is positioned with the seat back parallel to the sled deck and on top of the rails. A pneumatic system accelerates the sled system from the initial stationary position down the 23.75-m track. The target velocity at the seat is determined by the pressure used to accelerate the horizontal sled system. Honeycomb blocks, mounted on the barrier (Figure 7), are used to decelerate the seat fixture. Two snubbers (RCOS 3X 12 BS 04 Efdyn Inc., OK) are used to decelerate the

sled deck. A movable floor assembly produces an independent floor pulse. The 0.406- × 0.406- × 0.0063-m floor plate pulse duration is tuned with elastomers (GBA-20 MEPC Inc., IL) that also return some energy, allowing for floor velocities that exceed the incoming seat velocity. While the use of a decelerative sled allows for a greater range of peak velocities than the vertical system, the orientation of the body with respect to gravity does present some challenges, including difficulties in achieving alternate postures such as acute and obtuse that were tested elsewhere.

Seat cushions were utilized as described in Table 1. When a seat cushion was present, the surface of the cushion was covered with a layer of gaffer’s tape. Otherwise, the PMHS was placed directly upon the rigid surface of the seat.

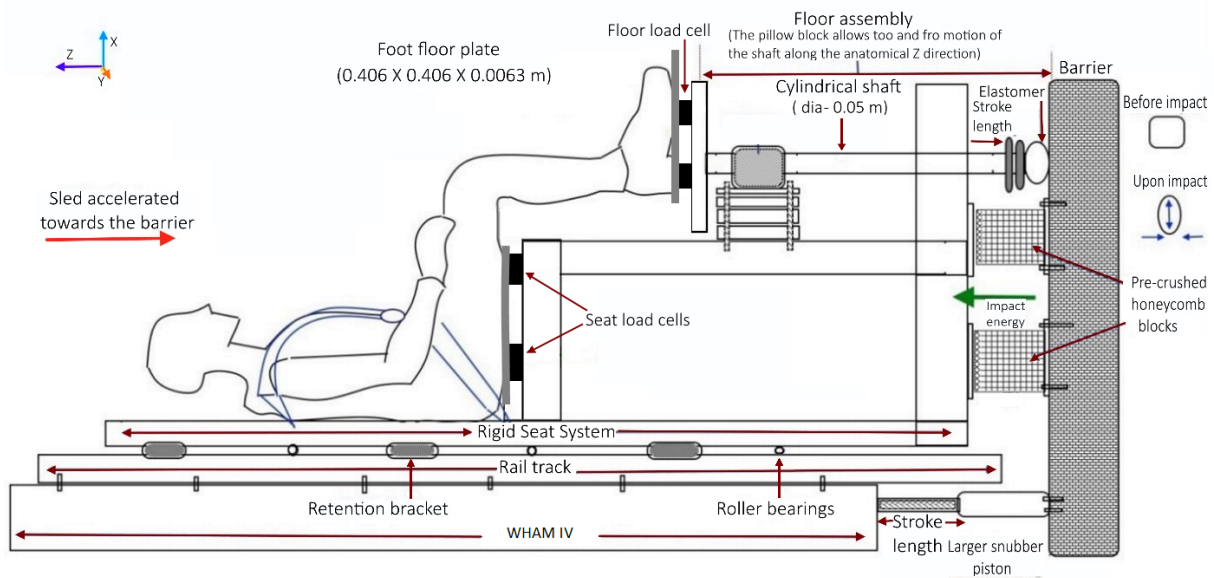


Figure 6. WSU horizontal sled system with the occupant positioned on the seat with a 5-point belt

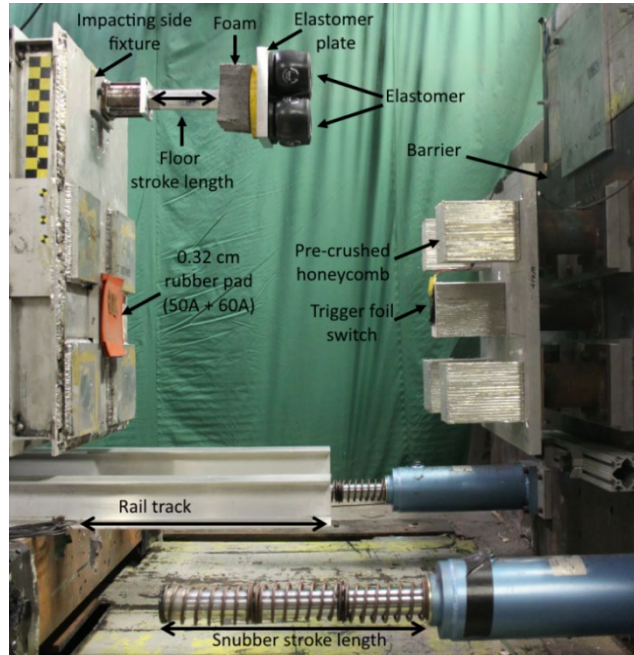


Figure 7. The two large-capacity snubbers mounted to the barrier are used to decelerate the sled deck, while the pre-crushed aluminum honeycomb blocks attached to the barrier are used to decelerate the seat fixture and produce a target TTP for the seat

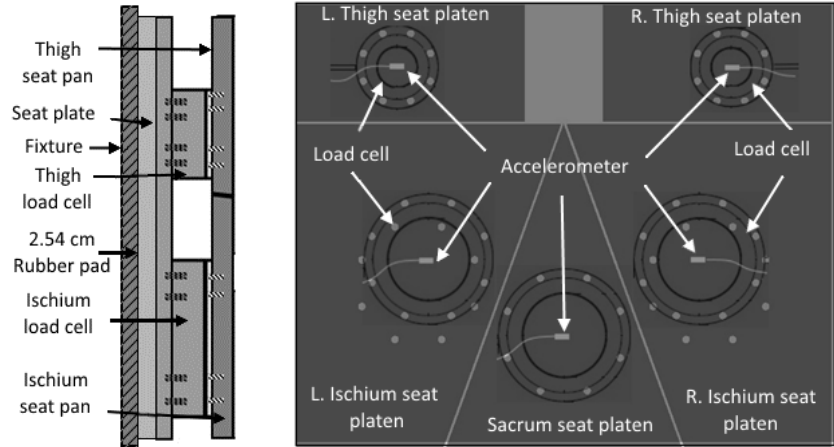
2.2.2 Instrumentation Locations and Transducer Types

The test fixture contained an array of uniaxial load cells and accelerometers at the occupant–seat and occupant–floor interfaces (Table 9 and Figure 8). The seat load cell configuration included uniaxial load cells at the sacrum plate, left and right ischium plates, and left and right thigh plates, allowing for an analysis of seat load distribution between the components (Rupp et al., 2016), as well as the ability to sum the individual loads to calculate a total seat force. Floor load cells and accelerometers measured the total floor force and floor acceleration. Each foot consisted of a separate fore- and hindfoot load cell–accelerometer pair, such that the components of floor load could be evaluated for each foot, as well as total loads. Fixture velocities were calculated by integrating acceleration signals.

Table 9. Masses and Instrumentation Used for Mass Compensation

Location	Plate Mass (kg)	Load Cell Names	Load Cell Model	Accelerometer Name	Accelerometer Model
Left heel	1.29	Hindfoot_Left	Interface LWPF1-50k	Hindfoot_Left	Endevco 72701A-20k
Right heel	1.29	Hindfoot_Right	Interface LWPF1-50k	Hindfoot_Right	Endevco 72701A-20k
Left forefoot	1.42	Forefoot_Left	Interface LWPF1-20k	Forefoot_Left	Endevco 72701A-6k
Right forefoot	1.42	Forefoot_Right	Interface LWPF1-20k	Forefoot_Right	Endevco 72701A-6k
Sacrum	1.90	Sacrum_Center	Interface LWPF1-50k	Seatpan_Sacrum	Endevco 72701A-20k
Left IT	2.97	Ischium_Left	Interface LWPF1-50k	Seatpan_Ischium_Left	Endevco 72701A-20k
Right IT	2.91	Ischium_Right	Interface LWPF1-50k	Seatpan_Ischium_Right	Endevco 72701A-20k
Left thigh	1.30	Femur_Left	Interface LWPF1-20k	Seatpan_Femur_Left	Endevco 72701A-6k
Right thigh	1.30	Femur_Right	Interface LWPF1-20k	Seatpan_Feumr_Right	Endevco 72701A-6k

Seat instrumentation:



Floor plate instrumentation:

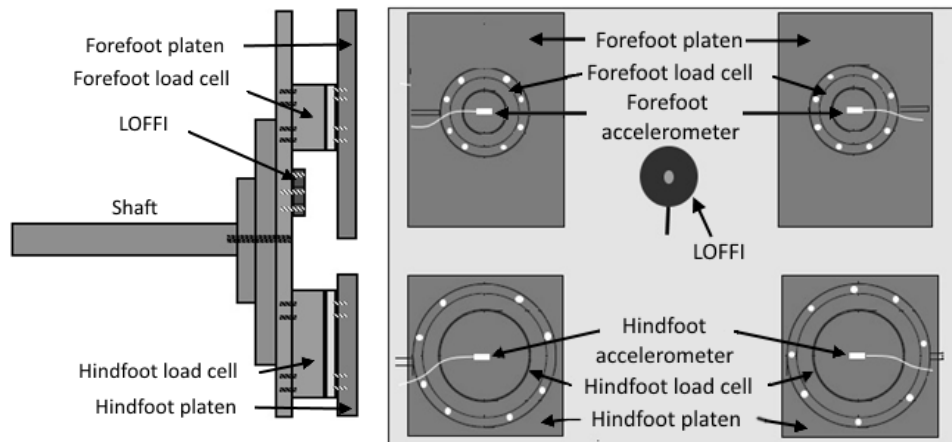


Figure 8. Rig instrumentation locations

The PMHS instrumentation included 6DOF sensors (6DX, Diversified Technical Systems, Inc., CA), uniaxial accelerometers (7270A, Endevco), acoustic emission sensors (Nano 30, Physical Acoustics Corporation, NJ), and uniaxial strain gauges (C2a-06-0621w-350, Vishay, NC). The types and locations of these sensors, and the orientations of strain gauges, are provided in Table 10 and Figure 9. The 6DX sensors measured X-, Y-, and Z-accelerations (A_x , A_y , and A_z , respectively) and X-, Y-, and Z-angular rates (AR_x , AR_y , and AR_z , respectively). The 6DX sensors were rigidly mounted to the skull (3 cm superior to the Frankfort Plane at the level of the trignon), the sternum, the thoracic vertebrae (T1, T5, T8, and T12), and the sacrum (S1–S3 level) using screws. The 6DX sensors were rigidly mounted to the right superior pubic ramus, the distal femurs, and the distal tibiae using worm gear clamps. The distal femur and tibia 6DX sensors were located proximal to the most distal portion of the bone at a distance of 0.2–0.3 and 0.15–0.25 of the total femur and tibia lengths, respectively. Linear accelerometers (7270A, Endevco, CA) (installed to measure A_z) were installed on the medial surface of the left and right calcaneus. A CT scan was conducted after instrumentation, but prior to testing, to document sensor positions relative to the skeleton.

Table 10. Subject Instrumentation Locations

6DX	Strain Gage*	Acoustic Emission Sensor	7270A Accelerometer
Head	Left ASIS	T4	Left Calcaneus
Sternum	Right ASIS	T7	Right Calcaneus
Right Superior Pubic Ramus	Left Superior Pubic Ramus	T9	
Left Distal Femur	Right Superior Pubic Ramus	T11	
Right Distal Femur	Left Distal Femur	L1	
Left Distal Tibia	Right Distal Femur	L2	
Right Distal Tibia	Left Proximal Tibia	L4	
T1	Right Proximal Tibia	Sacrum	
T5	Left Distal Tibia	Left Iliac Wing	
T8	Right Distal Tibia	Right Iliac Wing	
T12	Left Calcaneus	Left Calcaneus	
Sacrum (S1–S3)	Right Calcaneus	Right Calcaneus	

* Strain gauges were placed along the long axes of long bones, the circumferential direction of ribs, along the direction of the pelvic ring for the pubic ramus, along the direction of the iliac crest for the ASIS, and fore to aft for the calcaneus locations.

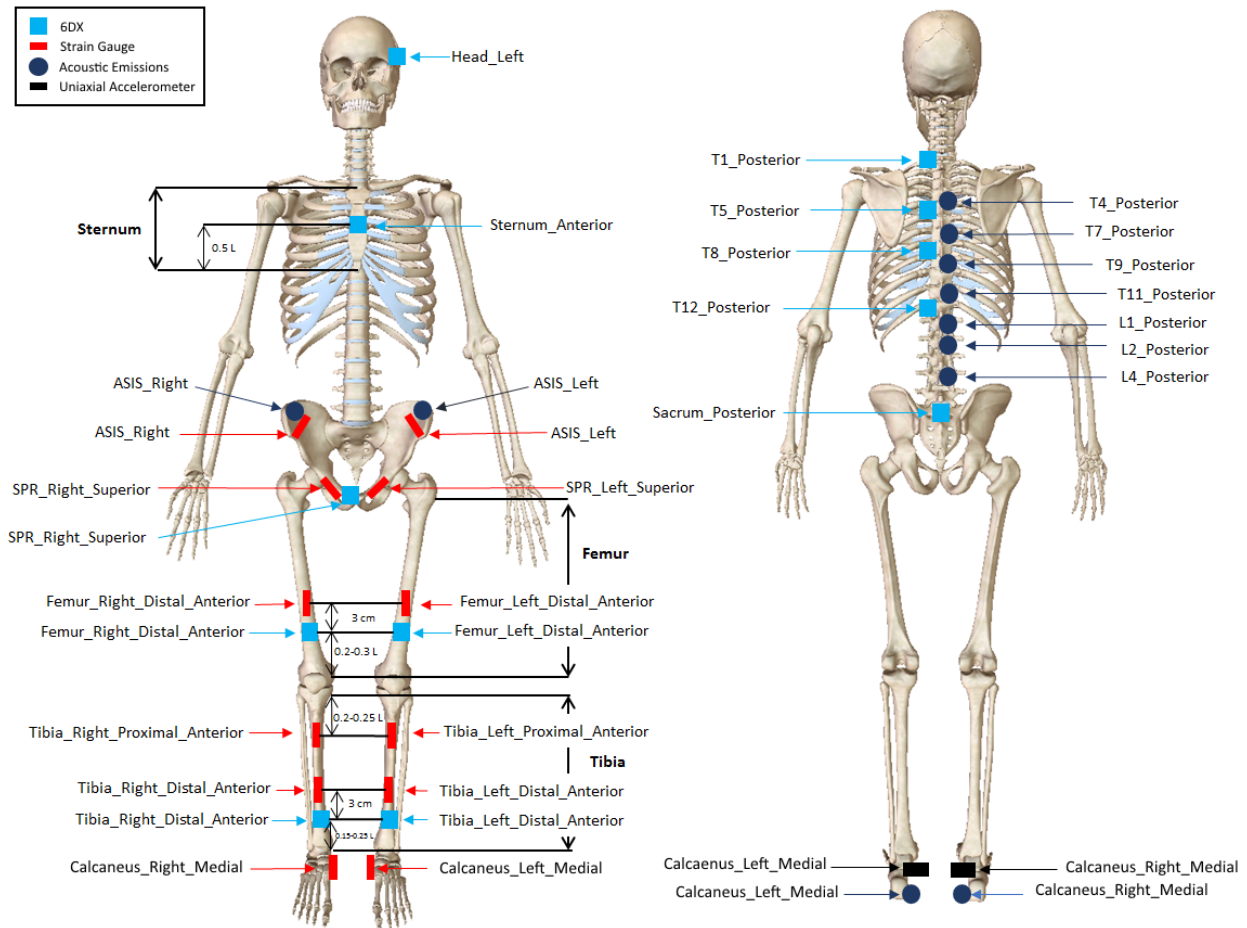


Figure 9. Subject instrumentation locations

2.2.3 Kinematic Analysis

Circular quadrant marker stickers (adhered to the surface of the bodysuit or PPE) were placed at various skeletal or surface landmarks for kinematic tracking. Tracked locations included the head (markers at the left and right trigion and left and right infraorbitale), shoulders (markers at the left and right acromion), knees (markers at the left and right patella, and left and right lateral femoral condyles), and boots (left and right forefoot, left and right hindfoot, left and right lateral malleolus) (Tables 11 through 13).

Various points on the fixture were tracked to define and translate the coordinate system as it moved through the camera frame (Table 14). Motion tracking and calibration were performed using motion analysis software (TEMA, Image Systems Motion Analysis).

Table 11. Surface Marker Anatomical Locations

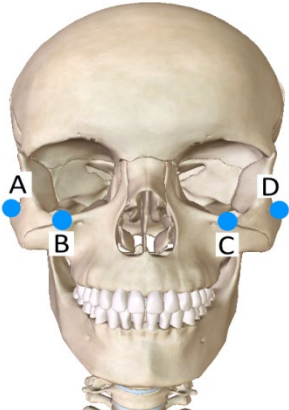
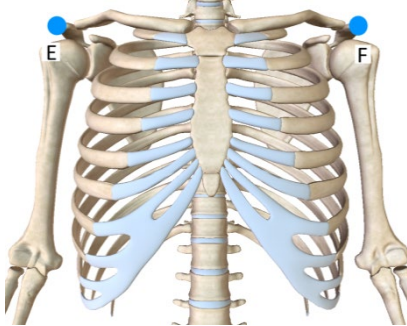
		
<p>A) Tragion_Right_Lateral B) Infraorbitale_Right C) Infraorbitale_Left D) Tragion_Left_Lateral</p>	<p>E) Acromion_Right_Lateral F) Acromion_Left_Lateral</p>	<p>G) Patella_Right_Anterior H) Epicondyle_Right_Lateral I) Malleolus_Right_Lateral J) Malleolus_Left_Lateral K) Epicondyle_Left_Lateral L) Patella_Left_Anterior</p>

Table 12. Surface Marker Boot Locations

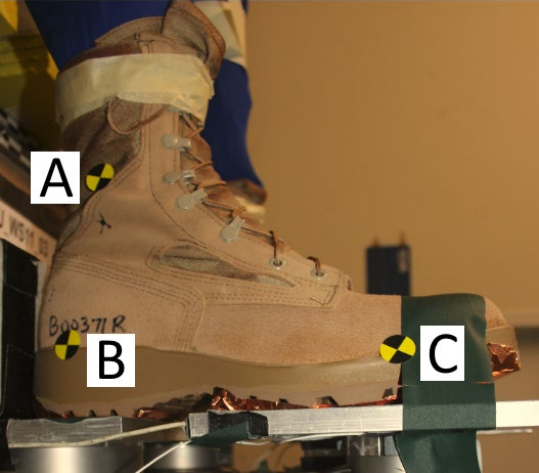
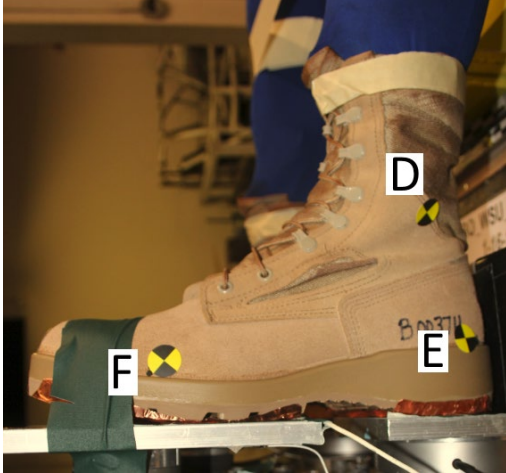
	
<p>A) Malleolous_Right_Lateral B) Boot_Hindfoot_Right_Lateral C) Boot_Forefoort_Right_Lateral</p>	<p>D) Malleolous_Left_Lateral E) Boot_Hindfoot_Left_Lateral F) Boot_Forefoort_Left_Lateral</p>

Table 13. Rig Kinematic Marker Locations

<p>A) Seatpan_Right_Top B) Seatpan_Right_Bottom C) Rig_Right D) Floor_Right*</p>	<p>E) Seatpan_Left_Top F) Seatpan_Left_Bottom G) Rig_Left H) Floor_Left *</p>

*Exact locations of floor plate fore-aft and up-down may vary between tests based on the femur and tibia length of the test subject.

Foot angle was calculated using the landmarks listed in Table 14.

Table 14. Calculated Kinematic Descriptions

Location	Description
Foot_Tibia_Right	Included angle between Epicondyle_Right_Lateral to Malleolus_Right_Lateral and Boot_Hindfoot_Right_Lateral to Boot_Forefoot_Right_Lateral
Foot_Tibia_Left	Included angle between Epicondyle_Left_Lateral to Malleolus_Left_Lateral and Boot_Hindfoot_Left_Lateral to Boot_Forefoot_Left_Lateral

2.2.4 Subject Characteristics

Table 15 provides the acceptance criteria for subjects tested by WSU for all PMHS experiments. All subjects were within predefined acceptable ranges, or received an exception from the sponsor. Standard subject anthropometry measured in accordance with reference document W0080, Minimum Pre-Test Anthropometry Requirements for Scaling (Rupp et al., 2016).

Table 15. Subject Acceptance Criteria

	Age (yrs)	Gender	Height (cm)	Weight (kg)	BMI	T-Score (L1-L4)
Acceptance Criteria	18	M	165	64	18	-1.0
	-		-	-	-	-
	80		186	106	35	+2.5

*S172105 subject with low mass was approved for use.

2.2.5 Subject Positioning

Subject positioning was based on the relative locations of skeletal surface landmarks, together with seated X-ray images. Figure 10 shows the target postures and highlights important joint angles and relative positions of landmarks for the example of a 90-90-90 posture. (Other postures utilized the same method with guidance from documented positioning methods [Rupp & Reed, 2015].) Landmarks were identified through palpation. Landmarks on the pelvis were determined through a lateral X-ray while seated on the test rig. Pelvis angle was defined as the angle of the line formed by the midpoint between the left and right ASISs (mid-ASIS) and the pubic symphysis landmark compared in reference to vertical.

A 3-D coordinate measurement device (Romer arm 7320I, Hexagon Metrology Inc., CA) was used to measure the position of the PMHS before each test. During the positioning process, 3-D coordinates were recorded for the specified landmarks and checked against target-relative coordinates. When landmarks fell outside of the tolerance, the PMHS was adjusted accordingly and remeasured until they were within tolerance; gaffer's and masking tape were used to secure each PMHS foot in the proper position against the floor plate by running a strip of tape from the PMHS booted forefoot to the floor plate. Tape mounting locations varied with each test (see Figure 10 for examples). Similarly, masking tape was used to secure PMHS knee spacing. All positioning tape was pre-cut, approximately 50% across immediately prior to each test such that the tape severed during the loading event. In all tests, all strips of tape were completely severed at the beginning of the loading event. Therefore, PMHS movement of the lower leg and feet did not appear to be influenced by the tape placement. In addition, foam blocks were used between the boot and test fixture, between the pelvis and test fixture, and between the head and test fixture to achieve the target positioning of key anatomical landmarks. These blocks were used for positioning to support the static mass of the body components. The kinematics of PMHS during testing were such that additional load was not applied to the blocks during the loading phase of the event. Final coordinates of anatomic landmarks were documented immediately prior to each test.

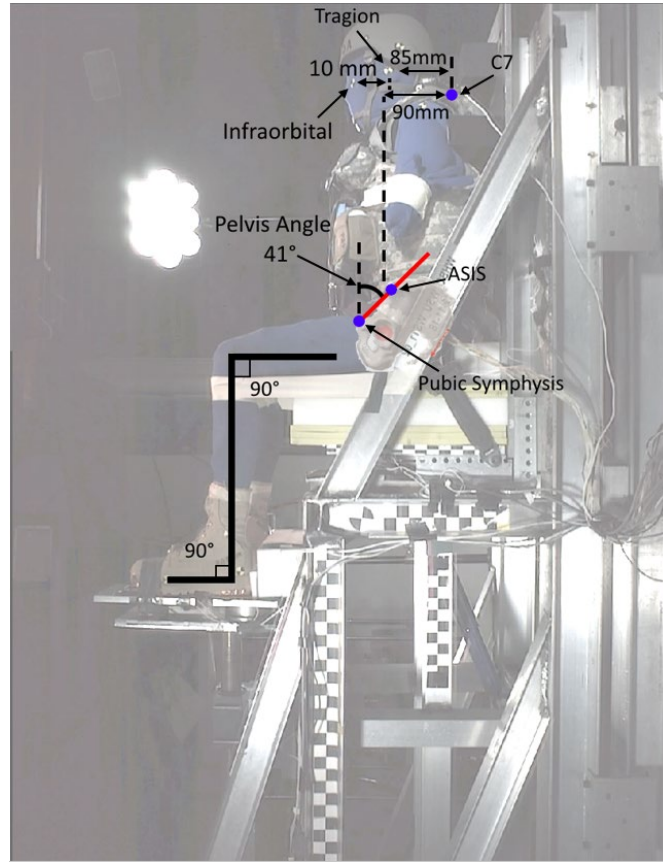


Figure 10. Target position

Target postures were based on the postures assumed by midsize male Soldiers seated in a military vehicle seat with a vertical back and horizontal seat cushion based on Reed and Ebert (2013). Positioning was performed following the procedure described by Rupp and Reed (2015). When positioning subjects, the highest priority was given to matching pelvis angle, head position and angle, and foot and knee angles. Lower priority was given to acromion position, as some subjects were missing forearms, preventing the use of the arm to control shoulder position.

2.2.6 Personal Protective Equipment, Boot, and Belt Fitting Procedures

PPE, including an ACH, IOTV, and Belleville 390 DES men's hot weather desert tan combat boots (Belleville Boot Company, Belleville, IL), were fitted to the PMHS in accordance with reference documents W00058 (Helmet Fitting Procedures [WIAMan Biomechanics Team, 2013a]), W0059 (IOTV Fitting Procedures [WIAMan Biomechanics Team, 2013b]), and W0060 (Boot Fitting Procedures [WIAMan Biomechanics Team, 2013c]), respectively. The routing and fitting of the 5-point seatbelt restraint harness was performed in accordance with reference document W0070 (Belt Fitting Procedures [WIAMan Biomechanics Team, 2013d]).

2.2.7 Data Processing

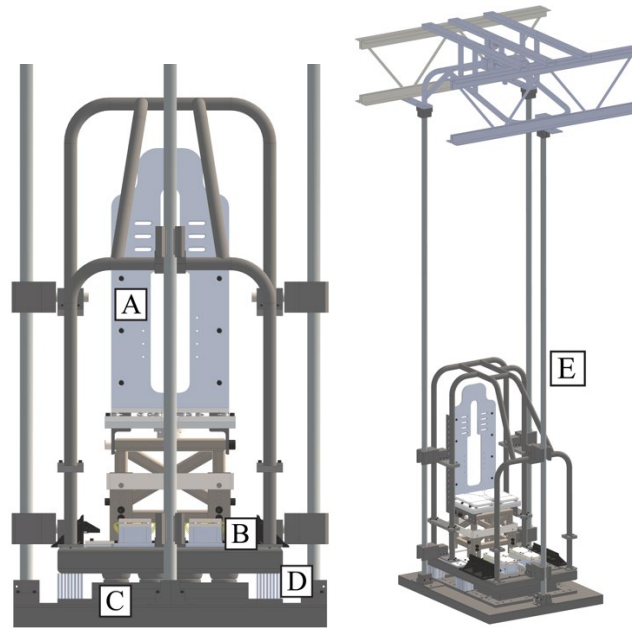
All signals were processed following the procedures used for BRC development, which include filtering with a low-pass 4th-order digital phaseless Butterworth filter. Accelerometers and seat/floor load cell data were filtered using a 3-dB cutoff frequency of 3 kHz. Angular rate data were filtered using a 3-dB cutoff frequency of 1650 Hz. DTS 6DX transducer measurements were transformed to standardized locations relative to skeletal anatomic landmarks using the procedure developed by SCoTT reported by Slykhouse et al. (2019).

TTP velocities for the floor and seat were calculated using the method defined by Spink (2014). This method involves a baseline shift and integration of the acceleration time history, the peak (largest negative) velocity within a time frame of interest, and identification of all local minima less than 90% of the absolute peak. The local minimum just prior to the absolute peak is selected as the new peak velocity and points corresponding to 5%, 20%, and 95% of the final peak velocity are determined. If the velocity history exhibits a monotonic fall between 5% and 20%, the velocity slope is calculated between the points at 5% and 95% of the peak velocity. If the velocity history is not monotonic between 5% and 20%, the data point immediately following the last positive derivative in the window is identified and used to replace zero as the baseline for the 5% calculation. The start and end times are determined by calculating the times at which the equation that defines the velocity slope are equal to zero and peak velocity, respectively. The TTP is the difference between the calculated ending and starting times.

2.3 University of Michigan Transportation Research Institute Test Rig

2.3.1 Test Fixture

The University of Michigan Transportation Research Institute (UMTRI) test fixture is a steel, vertical drop tower comprising a rigid seat with adjustable height and fore-aft displacement, and a decoupled footplate (Figure 11). The fixture is released from a specified height and accelerated by gravity onto aluminum honeycomb around the base of the fixture and elastomers beneath the footplate. The footplate was attached to the fixture using two nylon bolts designed to break away upon impact, which allowed the footplate to move freely relative to the fixture. The drop height, as well as the amount, type, and distribution of aluminum honeycomb and elastomers, controlled the deceleration pulse magnitude and duration at the seat and footplate.



- A) Seat system,
- B) Decoupled foot platform
- C) Linear elastomers
- D) Aluminum honeycomb
- E) Isometric view of primary platform

Figure 11. UMTRI test rig

Seat cushions were utilized as described in Table 1. When a seat cushion was present, the surface of the cushion was covered with a layer of gaffer's tape. Otherwise, the PMHS was placed directly upon the rigid surface of the seat.

2.3.2 Instrumentation Locations and Transducer Types

The test fixture contained an array of uniaxial load cells and accelerometers at the occupant–seat and occupant–footplate interfaces (Figure 12). A novel method of incorporating multiple piezoelectric load cells to support individual load sensing plates that may then be summed to evaluate the total load applied to a given plate was used, as described in Rupp et al. (2016). The seat load cell configuration included multiple load sensing plates at the sacrum, left and right ischium, and left and right thigh, allowing for an analysis of seat load distribution between the components, as well as the ability to sum the individual loads to calculate a total seat force (Rupp et al., 2016). Footplate load cells and accelerometers measured the total floor force and footplate acceleration. Force data were inertially compensated using acceleration data and the mass of the load cell plate (Table 16). Fixture velocities were calculated by integrating acceleration signals.

Table 16. Masses and Instrumentation Used for Mass Compensation

Location	Plate Mass (kg)	Load Cell Names	Load Cell Model	Accelerometer Name	Accelerometer Model
Left heel	3.36	Floor_Left_Aft_1-4	PCB_202B	Floor_Left_Aft	Endevco_72701A-20k
Right heel	3.36	Floor_Right_Aft_1-4	PCB_202B	Floor_Right_Aft	Endevco_72701A-20k
Left forefoot	1.2	Floor_Left_Fore_1-4	PCB_202B	Floor_Left_Fore	Endevco_7264D-2000
Right forefoot	1.2	Floor_Right_Fore_1-4	PCB_202B	Floor_Right_Fore	Endevco_7264D-2000
Sacrum	3.3	Seatpan_Center_Aft_1-4	PCB_203B	Seatpan_Center_Aft	Endevco_72701A-20k
Left IT	8.0	Seatpan_Left_Aft_1-6	PCB_203B	Seatpan_Left_Aft	Endevco_72701A-20k
Right IT	8.0	Seatpan_Right_Aft_1-6	PCB_203B	Seatpan_Right_Aft	Endevco_72701A-20k
Left thigh	3.3	Seatpan_Left_Fore_1-4	PCB_203B	Seatpan_Left_Fore	Endevco_7264D-2000
Right thigh	3.3	Seatpan_Right_Fore_1-4	PCB_203B	Seatpan_Right_Fore	Endevco_7264D-2000

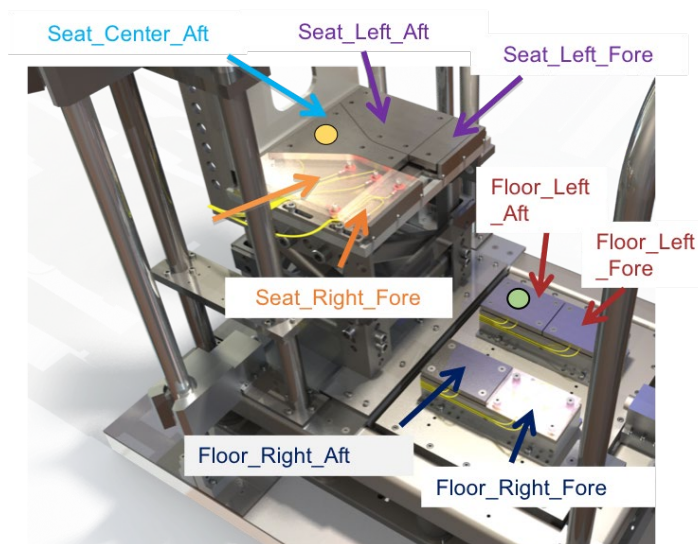


Figure 12. Rig instrumentation locations

PMHS instrumentation included 6DOF sensors (6DX, Diversified Technical Systems, Inc.), uniaxial accelerometers (7270A, Endevco), acoustic emission sensors (Nano 30, Physical Acoustics), and uniaxial strain gauges (CEA-06-250UN-350, Mirco-Measurements). The types and locations of these sensors, and the orientations of strain gauges are provided in Table 17 and Figure 13. The 6DX sensors measured X-, Y-, and Z-accelerations (A_x , A_y , and A_z , respectively)

and X-, Y-, and Z-angular rates (AR_x , AR_y , and AR_z , respectively). The 6DX sensors were rigidly mounted to the skull (3 cm superior to the Frankfort Plane at the level of the tragion) using Helicoil inserts and screws, thoracic vertebrae (T1, T5, T8, and T12), sacrum (S1–S3 level), left and right iliac wings, superior pubic rami, distal and proximal femurs, and distal and proximal tibias. The distal femur and tibia 6DX sensors were located proximal to the most distal portion of the bone at a distance of 0.2–0.3 and 0.15–0.25 of the total femur and tibia lengths, respectively. The proximal femur and tibia 6DX sensors were located distal to the most proximal portion of the bone at a distance of 0.2–0.3 and 0.2–0.25 of the total femur and tibia lengths, respectively. The 6DX sensors at the head, sternum, vertebral bodies, sacrum, and iliac wings were attached by rigid mounts installed in the bone via screws. The 6DX sensors at the pubic symphysis, femur, and tibia were installed via hose clamps tightened around the bone. The 7270A accelerometers (that measure A_z) were installed with a gel glue on the medial surface of the left and right calcaneus and oriented parallel to the leg long axis. A CT scan was conducted after instrumentation was installed, but prior to testing, to document sensor positions relative to the skeleton.

Table 17. Subject Instrumentation Locations

6DX	Strain Gage*	Acoustic Emission Sensor	7270A Accelerometer
Head	Left Rib 10	T4	Left Calcaneus
Sternum	Right Rib 10	T7	Right Calcaneus
Left Iliac Wing	Left ASIS	T11	
Right Iliac Wing	Right ASIS	L2	
Left Superior Pubic Ramus	Left Superior Pubic Ramus	L4	
Right Superior Pubic Ramus	Right Superior Pubic Ramus	Sacrum	
Left Proximal Femur	Left Proximal Femur	Left Iliac Wing	
Right Proximal Femur	Right Proximal Femur	Right Iliac Wing	
Left Distal Femur	Left Distal Femur	Left Calcaneus	
Right Distal Femur	Right Distal Femur	Right Calcaneus	
Left Proximal Tibia	Left Proximal Tibia		
Right Proximal Tibia	Right Proximal Tibia		
Left Distal Tibia	Left Distal Tibia		
Right Distal Tibia	Right Distal Tibia		
T1	Left Calcaneus		
T5	Right Calcaneus		
T8			
T12			
Sacrum (S1-S3)			

* Strain gauges were placed along the long axes of long bones, the circumferential direction of ribs, along the direction of the pelvic ring for the pubic ramus, along the direction of the iliac crest for the ASIS, and fore to aft for the calcaneus locations.

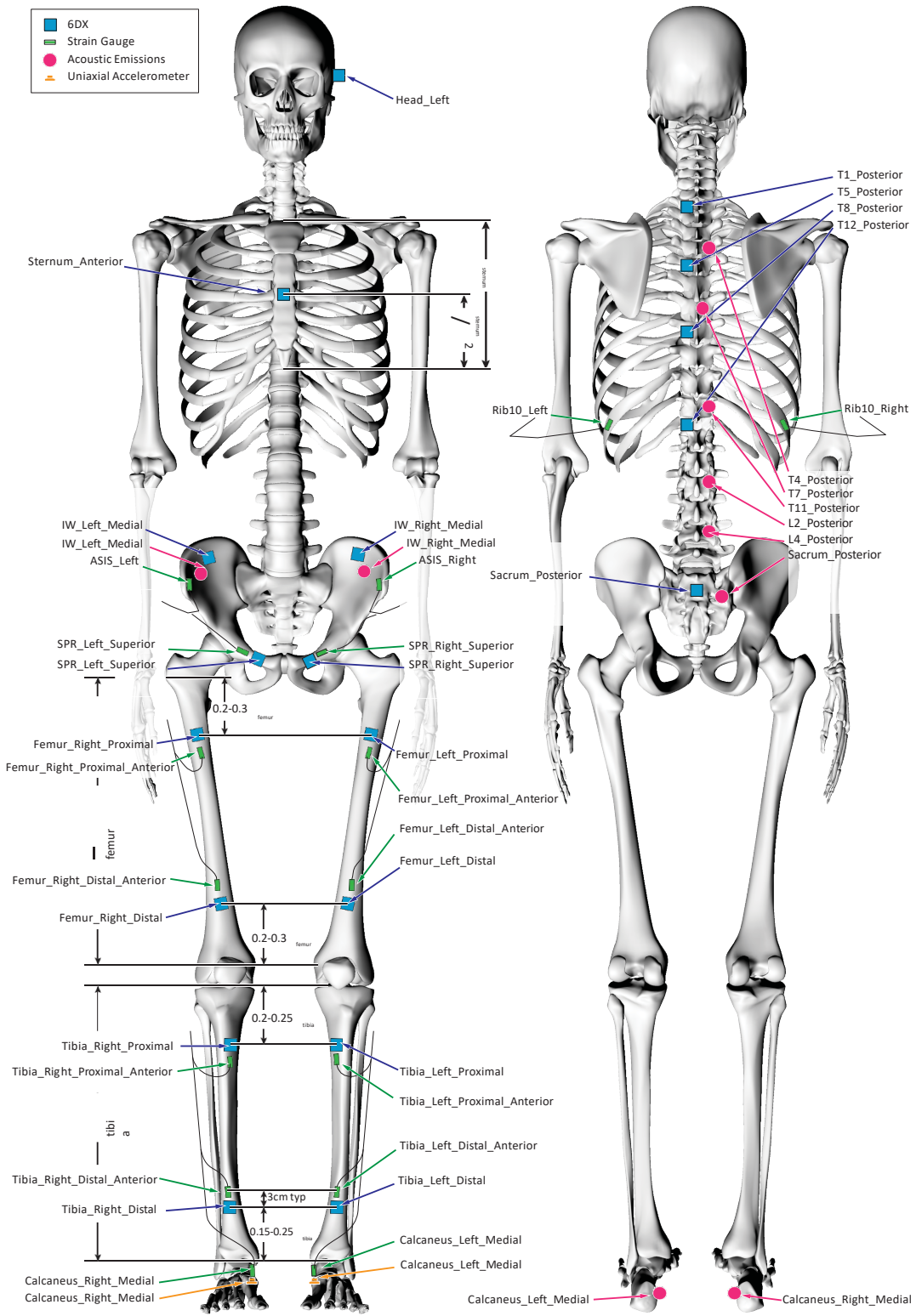


Figure 13. Subject instrumentation locations

2.3.3 Kinematic Analysis

Spherical markers (rigidly installed in bone) or quadrant marker stickers (adhered to the surface of clothing or PPE) were placed at various skeletal or surface landmarks for kinematic tracking. Tracked locations included the head (five spherical markers at various locations of the face), shoulders (spherical markers at left and right acromion), knees (spherical markers at left and right patella, quadrant markers at left and right lateral femoral condyle), and boots (left and right forefoot, left and right hindfoot, left and right lateral malleolus) (Tables 18 and 19). Various points on the fixture were tracked to define and translate the coordinate system as it moved through the camera frame (Table 20). Motion tracking and calibration were performed using motion analysis software (TEMA, Image Systems Motion Analysis).

Table 18. Rigidly Installed Kinematic Marker Locations

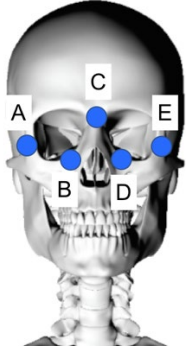
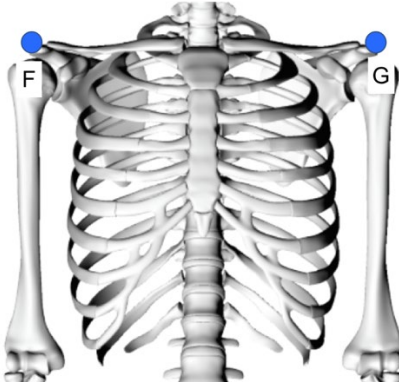
		
<p>A) Head_Anterior_Lateral_Right B) Head_Anterior_Medial_Right C) Head_Anterior_Medial D) Head_Anterior_Medial_Left E) Head_Anterior_Lateral_Left</p>	<p>F) Shoulder_Right_Lateral G) Shoulder_Left_Lateral</p>	<p>H) Knee_Right_Anterior I) Knee_Left_Anterior</p>

Table 19. Kinematic Surface Marker Locations

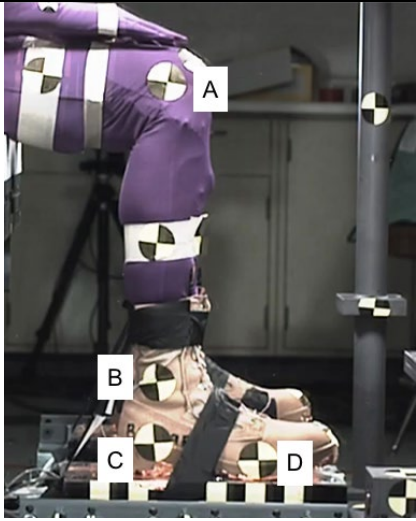
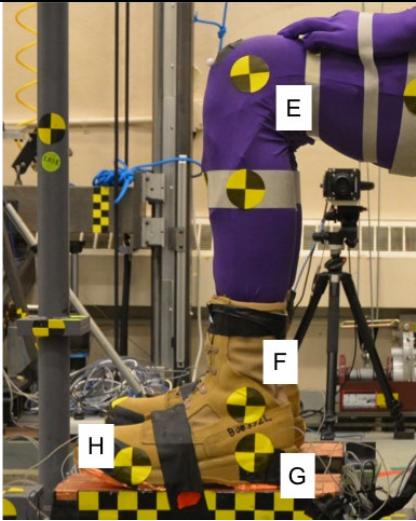
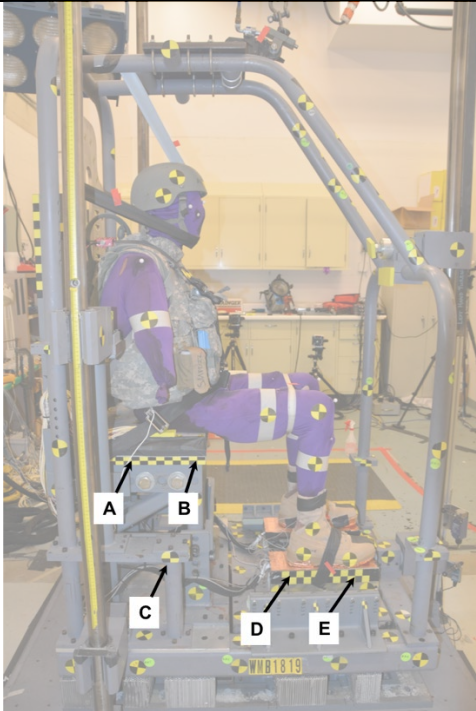
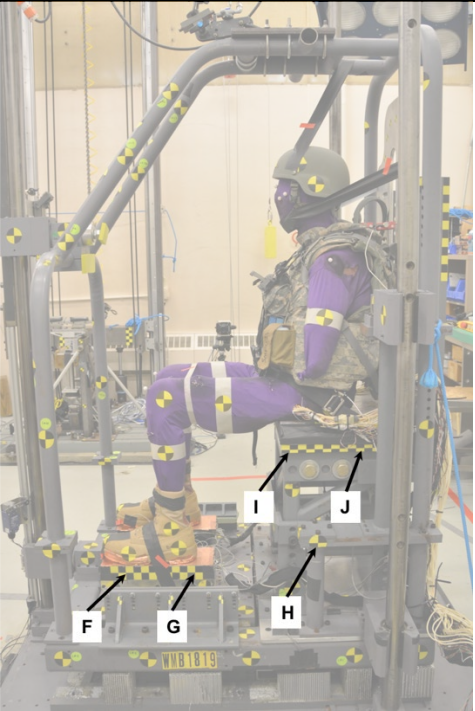
 A photograph of a right leg in a purple and white motion capture suit. Four white circular markers with black crosshairs are visible: marker A is on the lateral side of the knee; marker B is on the superior side of the right boot; marker C is on the posterior side of the right boot; and marker D is on the anterior side of the right boot.	 A photograph of a left leg in a purple and white motion capture suit. Four white circular markers with black crosshairs are visible: marker E is on the lateral side of the knee; marker F is on the superior side of the left boot; marker G is on the posterior side of the left boot; and marker H is on the anterior side of the left boot.
<p>A) Knee_Right_Lateral B) Boot_Right_Lateral_Superior C) Boot_Right_Lateral_Posterior D) Boot_Right_Lateral_Anterior</p>	<p>E) Knee_Left_Lateral F) Boot_Left_Lateral_Superior G) Boot_Left_Lateral_Posterior H) Boot_Left_Lateral_Anterior</p>

Table 20. Rig Kinematic Marker Locations

	
<p>A) Seatpan_Right_Aft* B) Seatpan_Right_Fore C) Rig_Right_Aft D) Floor_Right_Aft E) Floor_Right_Fore*</p>	<p>F) Floor_Left_Fore* G) Floor_Left_Aft H) Rig_Left_Aft I) Seatpan_Left_Fore* J) Seatpan_Left_Aft</p>

*Exact locations of seatpan aft and floor fore may vary between tests based on visibility from camera views.

The location of the head CG was calculated at each point in time using the skeletal surface markers shown in Table 18 based on the head CG location relative to these markers calculated using CT data with the procedure defined in the W0084 technical guidance document (Bass et al., 2016). For this calculation, it was assumed that head CG does not change over the course of the event. Foot angle was also calculated using the landmarks listed in Table 21.

Table 21. Calculated Kinematic Descriptions

Location	Description
Head_Center	Calculated position using a rigid body transformation from rigidly installed kinematic markers on head (Table 3) and head CG calculated from CT scan
Boot_Knee_Right	Included foot angle between Knee_Right_Lateral to Boot_Right_Lateral_Superior and Boot_Right_Lateral_Posterior to Boot_Right_Lateral_Anterior
Boot_Knee_Left	Included foot angle between Knee_Left_Lateral to Boot_Left_Lateral_Superior and Boot_Left_Lateral_Posterior to Boot_Left_Lateral_Anterior

2.3.4 Subject Characteristics

Table 22 provides the acceptance criteria for subjects tested by UMTRI for all PMHS experiments. All subjects were within predefined acceptable ranges, or received an exception from the sponsor. Standard subject anthropometry measured in accordance with reference document W0080, Minimum Pre-Test Anthropometry Requirements for Scaling (Bass et al., 2013).

Table 22. Subject Acceptance Criteria

Test Series ID	Age (yrs)	Gender	Height (cm)	Weight (kg)	BMI	T-Score (L1–L4)
Acceptance	18		165	64	18	-1.0
Criteria	-	M	-	-	-	-
	80		186	106	35	+2.5

*35249 L1–L5 T-score performed with QCT; approved for use by the WEO on 25 May 2017.

2.3.5 Subject Positioning

Subject positioning was based on the relative locations of skeletal surface landmarks, together with seated X-ray images. Figure 14 shows the target postures and highlights important joint angles and relative positions of landmarks for the example of a 90-90-90 posture. (Other postures utilized the same method with guidance from documented positioning methods [Rupp & Reed, 2015].) Landmarks were identified through palpation. Landmarks on the pelvis were determined through a lateral X-ray while seated on the test rig. Pelvis angle was defined as the angle of the line formed by the midpoint between the left and right ASISs (mid-ASIS) and the pubic symphysis landmark compared in reference to vertical.

A 3-D coordinate measurement device (FARO arm) was used to measure the position of the PMHS prior to each test. During the positioning process, 3-D locations were recorded at various landmarks and checked against target relative orientations. When measurements fell outside of tolerance, the PMHS was adjusted accordingly and remeasured until within tolerance or as close to the target range as PMHS anatomy permitted. Gaffer’s tape was used to secure each PMHS head in the proper position by running a strip or multiple strips of tape from the PMHS head and/or helmet to a rigid location on the test fixture. Tape mounting locations varied with each test, but tape was typically affixed to the PMHS chin, nose, or helmet (see Figure 14 for examples). For each PMHS, the fewest strips of tape that were sufficient to secure the head in the proper position were used. Tape was pre-cut approximately 90% across immediately prior to each test such that the tape severed during the loading event. In all tests, all strips of tape were completely severed at the beginning of the loading event. Therefore, PMHS movement of the head and feet did not appear to be influenced by the tape placement. Final coordinates were documented immediately prior to each test. A similar taping method was used to secure the feet prior to impact.

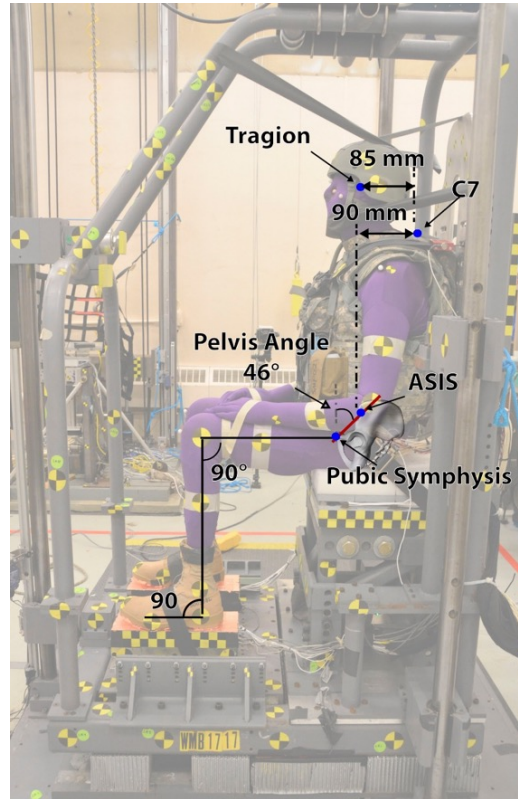


Figure 14. Target position

Target postures were based on the postures assumed by midsize male Soldiers seated in military vehicle seat with a vertical back and horizontal seat cushion angles based upon Reed and Ebert (2013). Positioning was performed following the procedure described by Rupp and Reed (2015). When positioning subjects, the highest priority was given to matching pelvis angle, head position and angle, and foot and knee angles. Lower priority was given to acromion position, as some subjects were missing forearms, preventing the use of the arm to control shoulder position.

2.3.6 Personal Protective Equipment, Boot, and Belt Fitting Procedures

PPE, including an ACH, IOTV, and Belleville 390 DES men's hot weather desert tan combat boots (Belleville Boot Company, Belleville, IL) were fitted to the PMHS in accordance with reference documents W0058 (Helmet Fitting Procedures [WIAMan Biomechanics Team, 2013a]), W0059 (IOTV Fitting Procedures [WIAMan Biomechanics Team, 2013b]), and W0060 (Boot Fitting Procedures [WIAMan Biomechanics Team, 2013c]), respectively. The routing and fitting of the 5-point seatbelt restraint harness was performed in accordance with reference document W0070 (Belt Fitting Procedures [WIAMan Biomechanics Team, 2013d]).

2.3.7 Data Processing

Similar to BRC development, accelerometers and individual seat/floor load cells were filtered using a low-pass 4th-order digital phaseless Butterworth filter using a cutoff frequency of 3 kHz.

Angular rate data were filtered using a cutoff frequency of 1650 Hz. As described in Section 2.3.2, individual uniaxial piezoelectric load cells attached to a given load sensing plate (illustrated in Figure 12) are summed to calculate hindfoot and forefoot loads, as well as loads applied to different parts of the pelvis and thighs. The high-frequency response and lack of damping in these load cells, coupled with the vibration produced by crushing aluminum honeycomb to generate the seat/floor pulses results in noise in the combined load cell data below 3 kHz; therefore, specific methods developed for this device are used where both the summed loads and the accelerometer used to inertially compensate these loads are filtered using a cutoff frequency of 1 kHz when combined. This method was confirmed during the development of this load sensing system. DTS 6DX transducer measurements were transformed to standardized locations relative to skeletal anatomic landmarks using the procedure developed by SCoTT reported by Slykhouse et al. (2019). Seat and floor velocities were calculated by integrating Z-axis accelerometers located under the center of the seat and under the center of the left and right feet.

TTP velocities for the floor and seat were calculated using the method defined by Spink (2014). This method involves a baseline shift and integration of the acceleration time history, the peak (largest negative) velocity within a time frame of interest and identification of all local minima less than 90% of the absolute peak. The local minimum just prior to the absolute peak is selected as the new peak velocity and points corresponding to 5%, 20%, and 95% of the final peak velocity are determined. If the velocity history exhibits a monotonic fall between 5% and 20%, the velocity slope is calculated between the points at 5% and 95% of the peak velocity. If the velocity history is not monotonic between 5% and 20%, the data point immediately following the last positive derivative in the window is identified and used to replace zero as the baseline for the 5% calculation. The start and end times are determined by calculating the times at which the equation that defines the velocity slope are equal to zero and peak velocity, respectively. The TTP is the difference between the calculated ending and starting times.

3. RESULTS

All data were first organized into tables. Key spinal injuries from each test were organized into groups by anatomy and Abbreviated Injury Scale (AIS) score as follow to identify trends:

Grouped Injury Levels:

- Pelvic ring
 - Excludes any sacrum-only pelvic fractures, unless the sacroiliac joint is involved.
- Sacrum
- Lumbar (L)-Spine (AIS2+)
 - Excludes any injuries that only involve the transverse process or spinous process.
- L-Spine (AIS3+)
- Thoracic (T)-spine (AIS2+)
 - Excludes any injuries that only involve the transverse process or spinous process.

Key peak input and response variables were also summarized with peak and TTP reported in accordance with methods described by Spink (2014). Graphical examples of peak and TTP calculations for seat force and sacrum velocity are illustrated in Figure 15.

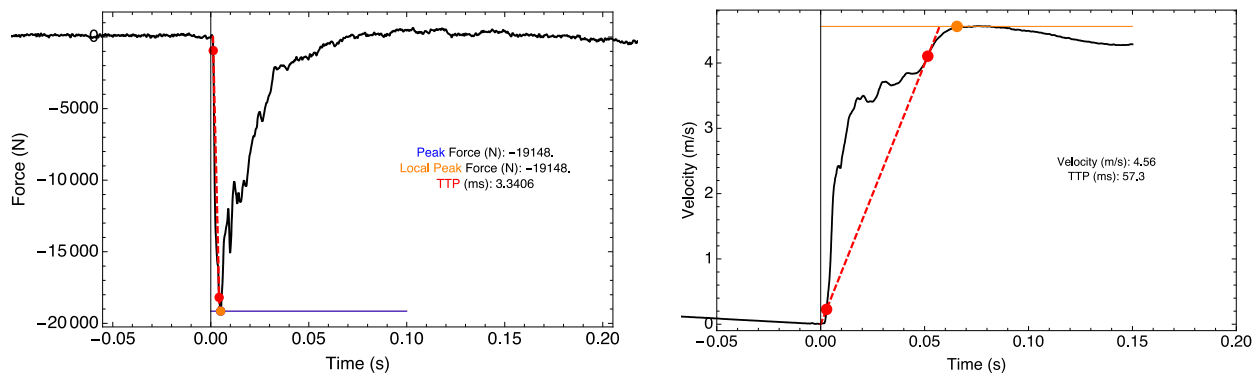


Figure 15. Peak seat Fz and sacrum velocity and TTP

The presence of seat padding and PPE were also summarized.

Injury summary tables for APL, WSU, and UMTRI are provided in Tables 23, 24, and 25, respectively.

Table 23. APL Injury Summary Table

Performer	APL																						
	WH01			WH03		WH04			WH08			WH12		WS04	WS10		WA01	WA04	WA06	WA07			
Series	BRC13011299	BRC13011317	BRC13122239	BRC12121219	S142237	15-09060	L141473	S150182	S150678	15-12028	15-10034	15-00441	S161437	1604013	S161490	S170374	16-10009	1612325R	F182258	S86A00988	OSU6673	S151345	S151697
Specimen ID	BRC13011299	BRC13011317	BRC13122239	BRC12121219	S142237	15-09060	L141473	S150182	S150678	15-12028	15-10034	15-00441	S161437	1604013	S161490	S170374	16-10009	1612325R	F182258	S86A00988	OSU6673	S151345	S151697
T-Spine AIS2+	0	0	0	0	1	0	0	0	0	0	0	1	0	0	0	1	1	1	1	0	1	1	0
L-Spine AIS3+	0	0	0	0	0	0	0	0	0	0	0	0	0	0	0	0	1	0	0	0	0	0	1
L-Spine AIS2+	0	0	0	1	0	0	0	0	0	1	0	0	0	0	0	1	1	1	1	0	0	1	1
Sacrum	0	0	0	0	0	0	0	1	0	1	0	0	0	0	0	1	1	1	1	0	1	0	0
Pelvic Ring	0	0	0	0	0	0	0	1	0	0	0	0	0	0	0	0	1	0	1	0	1	0	0
Peak Seat Fz (kN)										-10.7	-15.9	-11.7					-33.8	-35.4					
Seat Fz TTP (ms)										20.1	16.0	24.9					12.4	11.6					
Peak Sacrum Vr (m/s)	4.0	4.5	5.1	4.9	3.7	4.5	4.6	5.3	4.2	5.2	4.5	4.3	4.3	5.3	5.1	6.5			10.3	3.2	5.9	7.2	6.4
Sacrum Vr TTP (ms)	15.0	25.6	31.9	39.7	11.9	16.6	27.2	67.8	23.6	36.4	35.7	33.8	75.6	70.1	72.0	37.7			53.5	17.9	12.4	31.6	41.5
Target Peak Seat Vz (m/s)	4	4	4	4	4	4	4	4	4	4	4	4	3	3	3	6	10	10	10	3	6	6	6
Target Seat Vz TTP (ms)	5	5	5	10	10	10	10	10	10	30	30	30	8	8	8	20	7.5	7.5	7.5	5	10	10	10
Target Peak Floor Vz (m/s)	4	4	4	6	6	6	6	6	6	8	8	8	8	8	8	8.5	15.5	15.5	15.5	3	8	8	8
Target Floor Vz TTP (ms)	5	5	5	5	5	5	5	5	5	2	2	2	2	2	2	2.5	2.5	2.5	2.5	5	5	5	5
Padding	r	r	r	r	r	r	r	r	r	r	r	r	OEM	OEM	OEM	r	V10	V10	V10	r	r	Eth	V1
PPE	B	B	B	B	B	B	M	M	M	M	M	M	M	M	M	M	M	M	M	B	B	B	M

1 = Injury at specified level
 0 = No Injury at specified level

r = Rigid Seat
 Padded seat

B = Boots Only
 M = Medium PPE

More Severe
 (higher force/velocity; shorter TTP)

Intermediate Severity
 (Color Gradient)

Less Severe
 (lower force/velocity; longer TTP)

Table 24. WSU Injury Summary Table

Performer	WSU													
	WH01		WH03		WH04			WH06			WA03	WS09		WS11
Series	OSU6725	OSU6908	LMD14-00355	S150758	S151176	S151317	LL15-10028	LL16-01011	LL16-02045	BRC13122202	S160712	L171491	S160979	S172105
Specimen ID	OSU6725	OSU6908	LMD14-00355	S150758	S151176	S151317	LL15-10028	LL16-01011	LL16-02045	BRC13122202	S160712	L171491	S160979	S172105
T-Spine AIS2+	1	0	0	1	0	0	0	0	0	1	1	1	1	1
L-Spine AIS3+	0	0	0	0	0	0	0	0	0	0	0	0	1	0
L-Spine AIS2+	0	1	1	0	0	0	1	0	0	0	0	0	1	0
Sacrum	1	0	0	0	1	0	0	0	0	0	1	1	0	0
Pelvic Ring	0	0	0	0	0	0	0	0	0	1	1	0	0	0
Peak Seat Fz (kN)							-9.5	-9.6	-6.9		-44.2	-21.2	-23.8	-18.4
Seat Fz TTP (ms)							37.0	29.4	36.6		9.2	4.1	14.1	11.1
Peak Sacrum Vr (m/s)	4.3			5.6	4.5	4.3	3.8	4.2	4.7	6.3	11.0	7.9	8.9	8.3
Sacrum Vr TTP (ms)	18.0			10.9	64.8	62.7	56.6	38.1	44.5	14.5	13.0	27.7	43.7	25.0
Target Peak Seat Vz (m/s)	4	4	4	4	4	4	4	4	4	6	12	9	9	9
Target Seat Vz TTP (ms)	5	10	10	10	10	10	55	55	55	5	5	5	5	5
Target Peak Floor Vz (m/s)	4	6	6	6	6	6	8	8	8	6	16.5	13.5	13.5	13.5
Target Floor Vz TTP (ms)	5	5	5	5	5	5	2	2	2	5	2	2.5	2.5	2.5
Padding	r	r	r	r	r	r	r	r	r	r	Eth	V10	V10	V10
PPE	B	B	B	M	M	M	M	M	M	B	M	M	M	M

1 = Injury at specified level
 0 = No Injury at specified level

r = Rigid Seat
 Padded seat

B = Boots Only
 M = Medium PPE

More Severe
 (higher force/velocity; shorter TTP)

 Intermediate Severity
 (Color Gradient)

 Less Severe
 (lower force/velocity; longer TTP)

Table 25. UMTRI Injury Summary Table

Performer	UMTRI																			
	WH01	WH02				WH07			WH11			WA02	WA05	WA08	WA09	WS01		WS12		
Series	6600	14-00364	6899	6944	S150268	15-12011	16-01020	35064	16-07027	16-08019	S161495	6858	15-00396	15-08052	34910	35286	S161876	35249	L162663	L170249
Specimen ID	6600	14-00364	6899	6944	S150268	15-12011	16-01020	35064	16-07027	16-08019	S161495	6858	15-00396	15-08052	34910	35286	S161876	35249	L162663	L170249
T-Spine AIS2+	1	0	0	0	0	1	1	0	1	1	1	1	0	0	0	1	1	0	1	1
L-Spine AIS3+	0	0	0	0	0	0	0	0	0	0	0	0	1	1	1	0	1	0	1	0
L-Spine AIS2+	1	1	0	0	0	0	0	1	1	0	1	1	1	1	1	1	1	0	1	0
Sacrum	0	0	1	1	1	1	1	1	0	0	0	1	0	0	1	0	1	1	1	1
Pelvic Ring	0	0	0	0	0	0	0	0	0	0	0	0	0	0	0	0	0	1	0	1
Peak Seat Fz (kN)	-19.1	-19.0	-18.0	-18.0	-14.7	-12.5	-15.4	-12.4	-11.9	-14.5	-14.0	-24.8	-12.2		-15.4	-18.7	-20.9	-29.5	-30.8	-28.5
Seat Fz TTP (ms)	3.3	1.5	3.9	3.7	4.0	21.5	29.5	23.9	18.8	19.6	19.8	9.8	9.7		19.8	14.5	15.7	6.4	6.4	5.5
Peak Sacrum Vr (m/s)	4.6	3.7	4.9	5.0	3.8	4.0	4.5	4.8	5.2	5.9	5.3	6.5	7.0	6.7	5.4	6.2	6.4	7.2	6.5	7.0
Sacrum Vr TTP (ms)	57.3	42.5	47.0	54.7	38.9	29.5	33.0	56.9	41.9	52.8	63.2	33.7	53.7	23.7	61.8	20.1	50.6	51.7	13.1	25.8
Target Peak Seat Vz (m/s)	4	4	4	4	4	4	4	4	5	5	5	6	6	6	5	6	6	6.5	6.5	6.5
Target Seat Vz TTP (ms)	5	5	5	5	5	40	40	40	10	10	10	10	10	10	10	5	5	7.5	7.5	7.5
Target Peak Floor Vz (m/s)	4	4	4	4	4	7	7	7	7.5	7.5	7.5	8	8	8	8	8.5	8.5	9	9	9
Target Floor Vz TTP (ms)	5	5	5	5	5	2.75	2.75	2.75	2.5	2.5	2.5	5	5	5	2.5	2.5	2.5	2.5	2.5	2.5
Padding	r	r	r	r	r	r	r	r	V10	V10	V10	r	Eth	V1	V10	Eth	Eth	r	r	r
PPE	B	M	M	M	M	M	M	M	M	M	M	B	B	B	M	M	M	M	M	M

1 = Injury at specified level
 0 = No Injury at specified level

r = Rigid Seat
 Padded seat

B = Boots Only
 M = Medium PPE

More Severe
 (higher force/velocity; shorter TTP)
 Intermediate Severity
 (Color Gradient)
 Less Severe
 (lower force/velocity; longer TTP)

3.1 Effects of Padding, Seat Pulse, and Pelvis Response on Pelvis/Spine Injury

In the analysis of injuries initiated by seat loading, the relationship between total seat force and the duration of loading as represented by TTP of seat loading were investigated. First, injuries that disrupted the pelvic ring at any point about its circumference were plotted against peak seat force and TTP of seat loading, as shown in Figure 16. No trend in pelvic injuries was observed with regard to TTP. However, injuries were observed to occur above 30 kN of seat force, although not in all tests shown. It was noted that these increased seat loads were all associated with short-duration pulses, but there is no indication that duration is a factor in the injuries. The effects of a padded seat cushion were not obvious from these data. Peak sacrum velocity and the TTP of sacrum velocity were also plotted for these tests, as shown in Figure 17. Pelvic ring injuries are observed in these tests with increased peak seat velocity across the range of TTPs tested. However, data suggest that no clear relationship exists between pelvic ring injury and TTP, as injurious and noninjurious tests cover the full range of TTP that was tested.

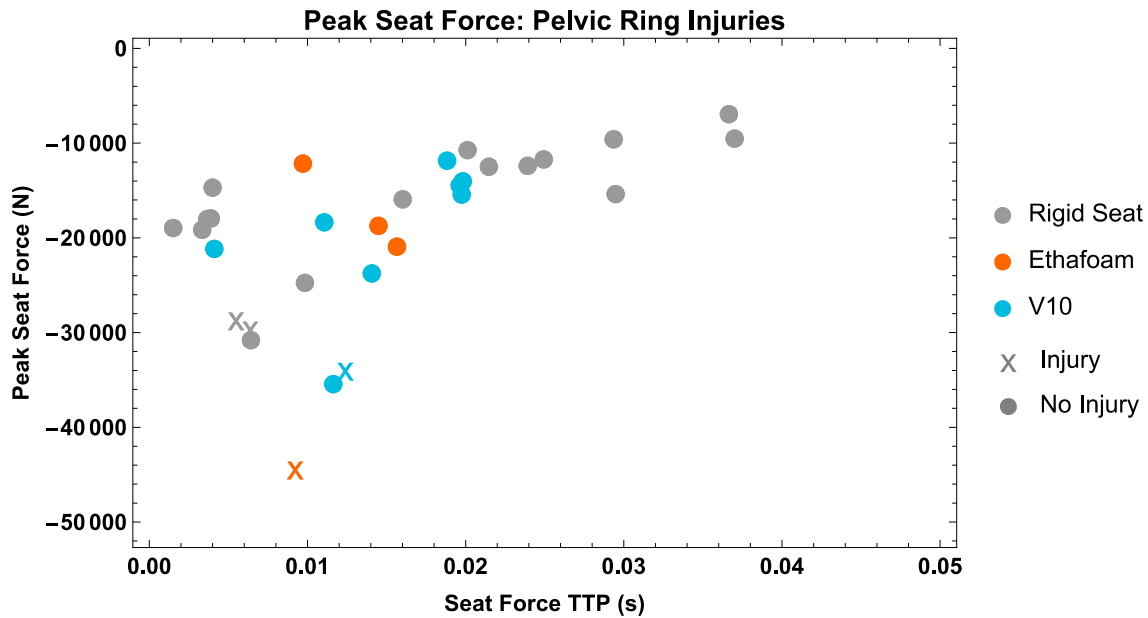


Figure 16. Effects of peak seat loads on pelvic ring injuries

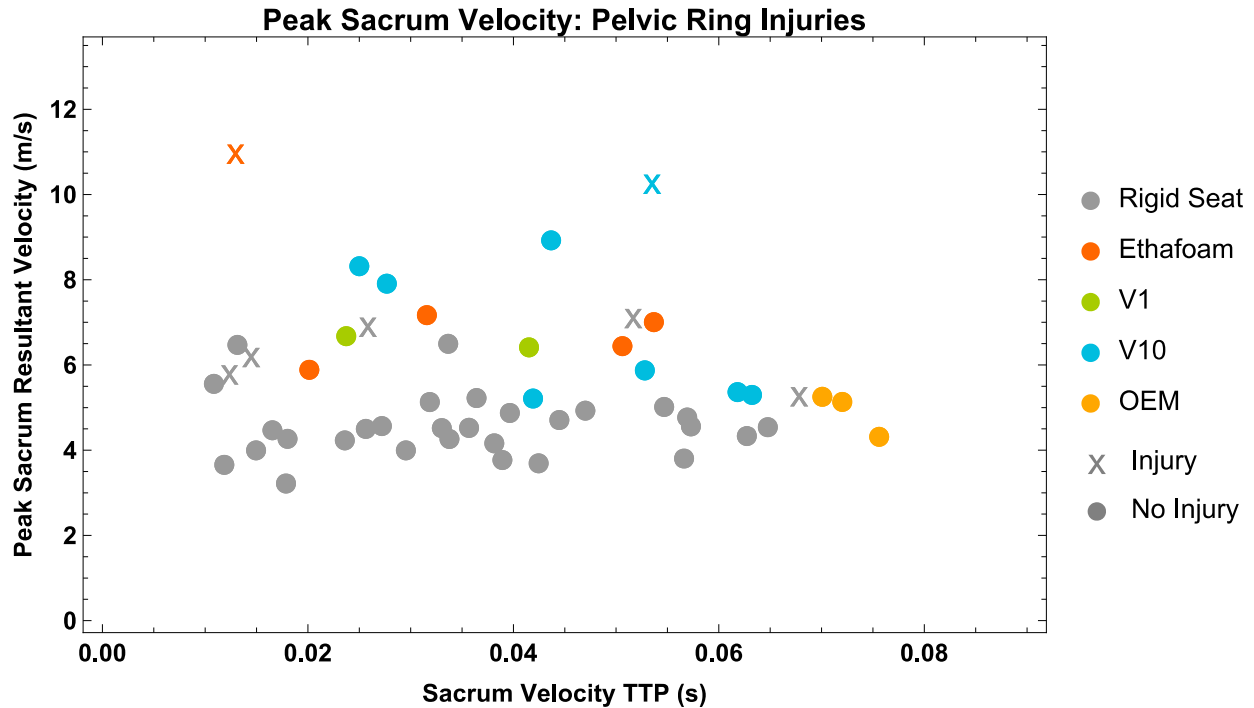


Figure 17. Effects of peak sacrum velocity on pelvic ring injuries

Similarly to the preceding analysis of pelvic ring injuries, injuries to the sacrum were also evaluated relative to seat loading, as shown in Figure 18. Sacrum injuries were observed to occur at all levels of loading and TTP, but were present in all tests with a shorter duration of approximately 10 ms and increased loads above 30 kN. Rigid seat interactions did not demonstrate a clear relationship with sacrum fractures for increased seat loads over 30 kN. Yet, the majority of coccyx fractures below 30 kN were in rigid seats (i.e., all but three injuries). As with pelvic ring injuries, peak pelvis velocity as shown in Figure 19 was less able to distinguish injurious from noninjurious conditions based upon either the magnitude or TTP of the peak pelvis velocity.

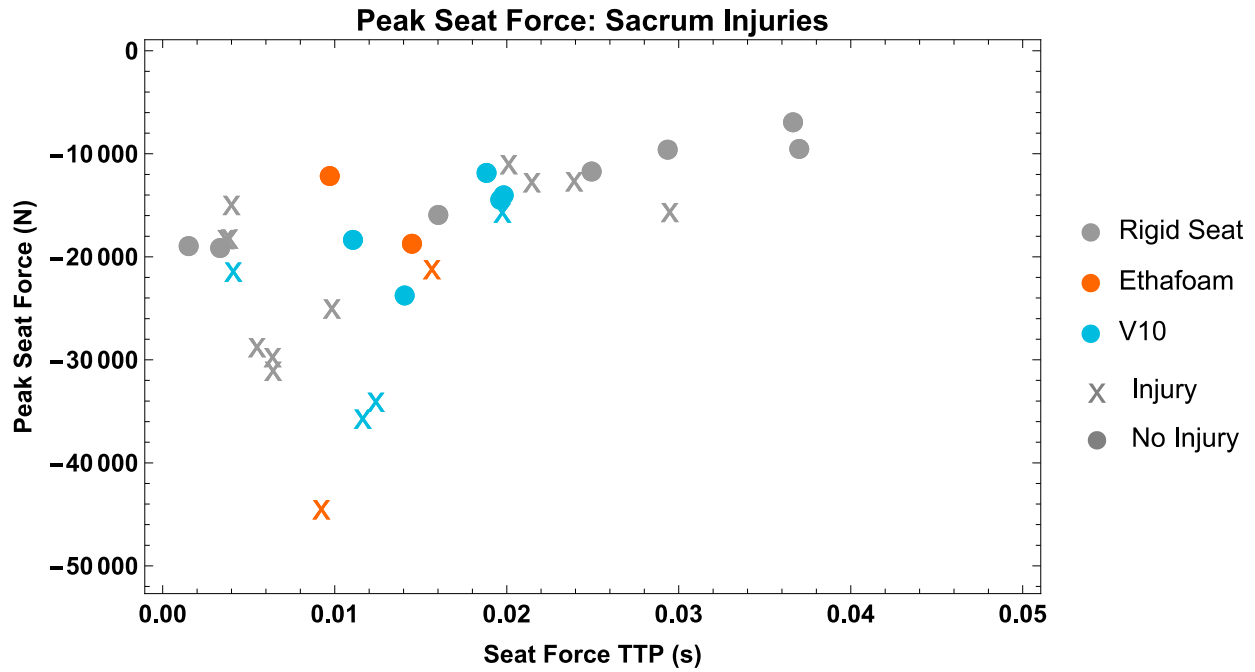


Figure 18. Effects of peak seat loads on sacrum injuries

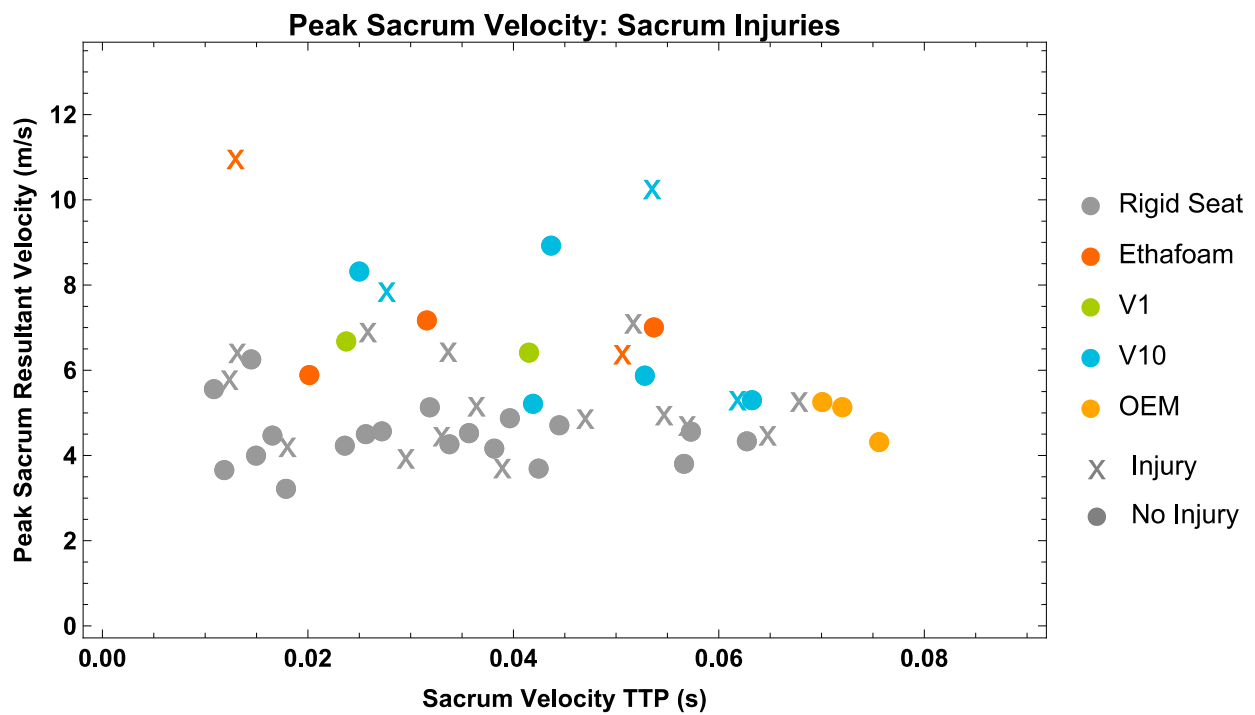


Figure 19. Effects of peak sacrum velocity on sacrum injuries

Injuries observed in the lumbar spine were grouped as either AIS2+ or AIS3+, which were plotted against seat loads in Figures 20 and 22, respectively. AIS2+ lumbar injuries are a subset of AIS3+ injuries that were drawn from the same group of experiments. Comparing the two plots, all lumbar injuries that fell above an approximate threshold of 20-kN seat load were categorized AIS3+. (Note that two additional AIS3+ injuries were associated with seat loads of less than 20 kN.) Five of the seven AIS2+ injuries that did not again appear as AIS3+ were in rigid seats, suggesting the potential effectiveness of padding in the mitigation of lumbar injuries due to UBB loading. AIS2+ and AIS3+ injuries were then plotted against peak sacrum velocity in Figures 21 and 23, respectively. As with pelvic and sacral injuries, peak resultant pelvis velocity was unable to differentiate between injurious and noninjurious conditions based upon either magnitude or TTP. Data do not suggest that a threshold of injury can be defined by peak pelvis velocity.

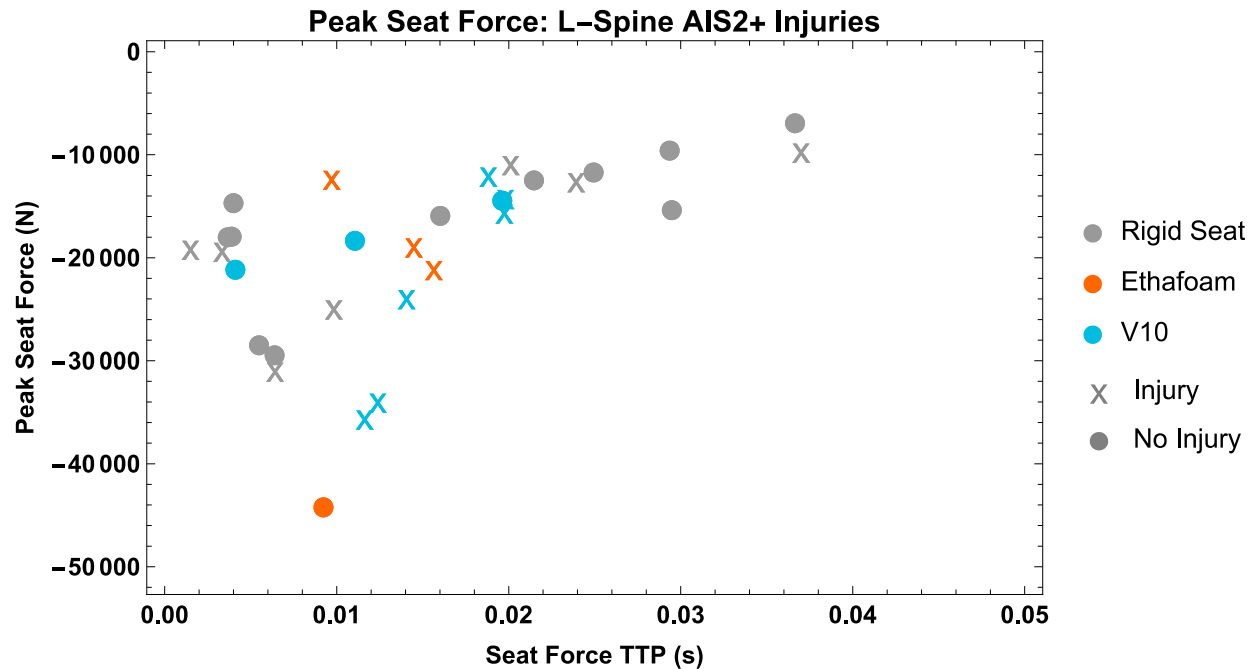


Figure 20. Effects of peak seat loads on AIS2+ lumbar spine injuries

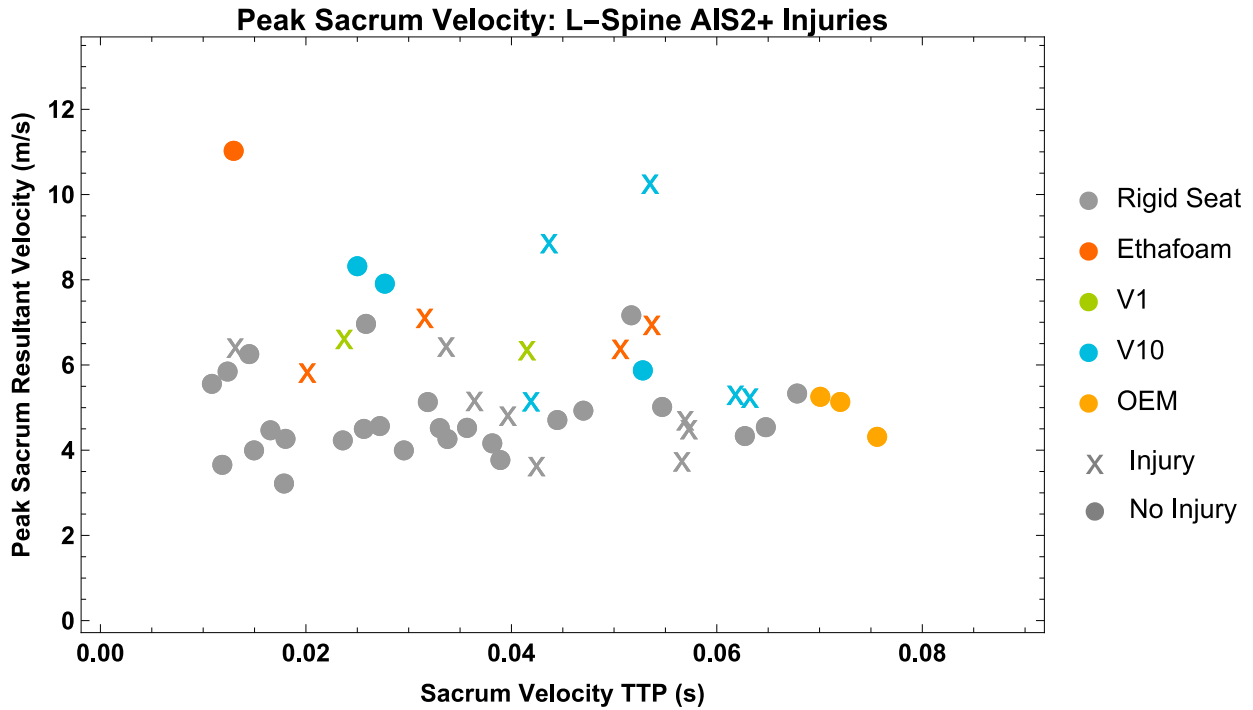


Figure 21. Effects of peak sacrum velocity on AIS2+ lumbar spine injuries

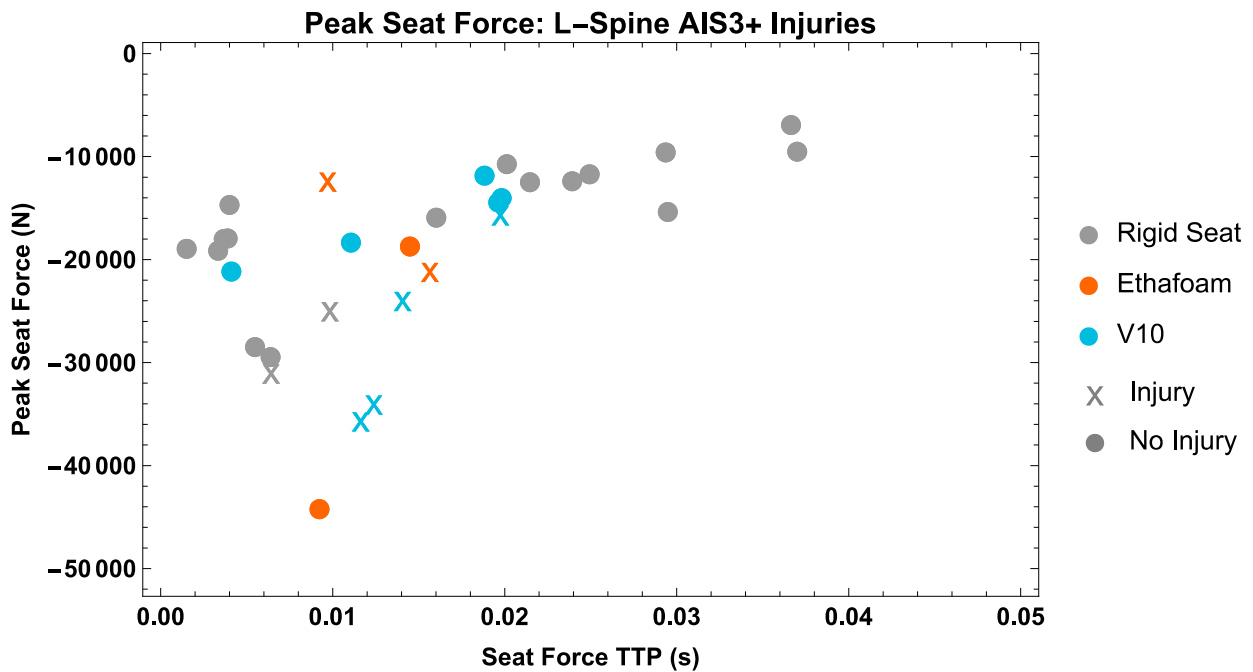


Figure 22. Effects of peak seat loads on AIS3+ lumbar spine injuries

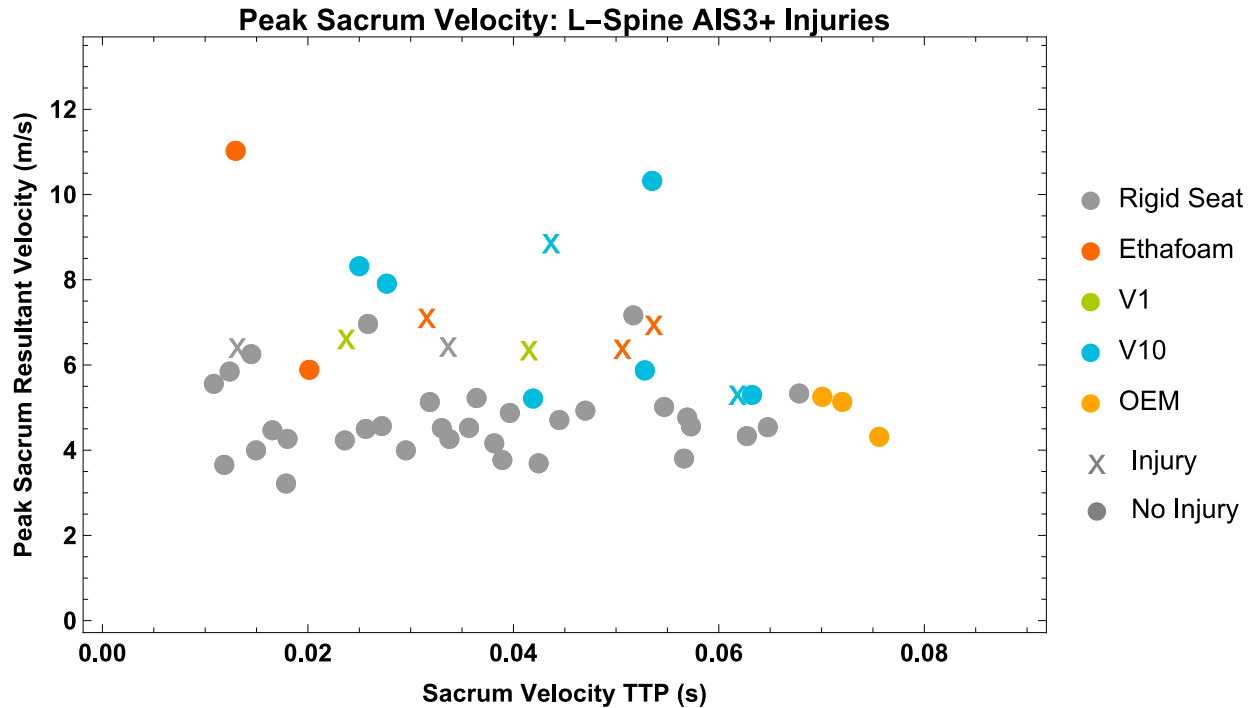


Figure 23. Effects of peak sacrum velocity on AIS3+ lumbar spine injuries

Finally, AIS2+ injuries of the thoracic spine were plotted against seat loads in Figure 24. These injuries were observed in 9 of the 10 tests with a peak seat load of 20 kN or greater, which suggests a high likelihood of concomitant thoracic spine injuries with lumbar injuries. No strong relationship between the use of a seat cushion and injury to the thoracic spine was observed. Again, results were plotted against peak sacrum velocity in Figure 25. As before, neither peak sacrum velocity nor TTP was able to differentiate either injury from noninjury or rigid from padded seat conditions.

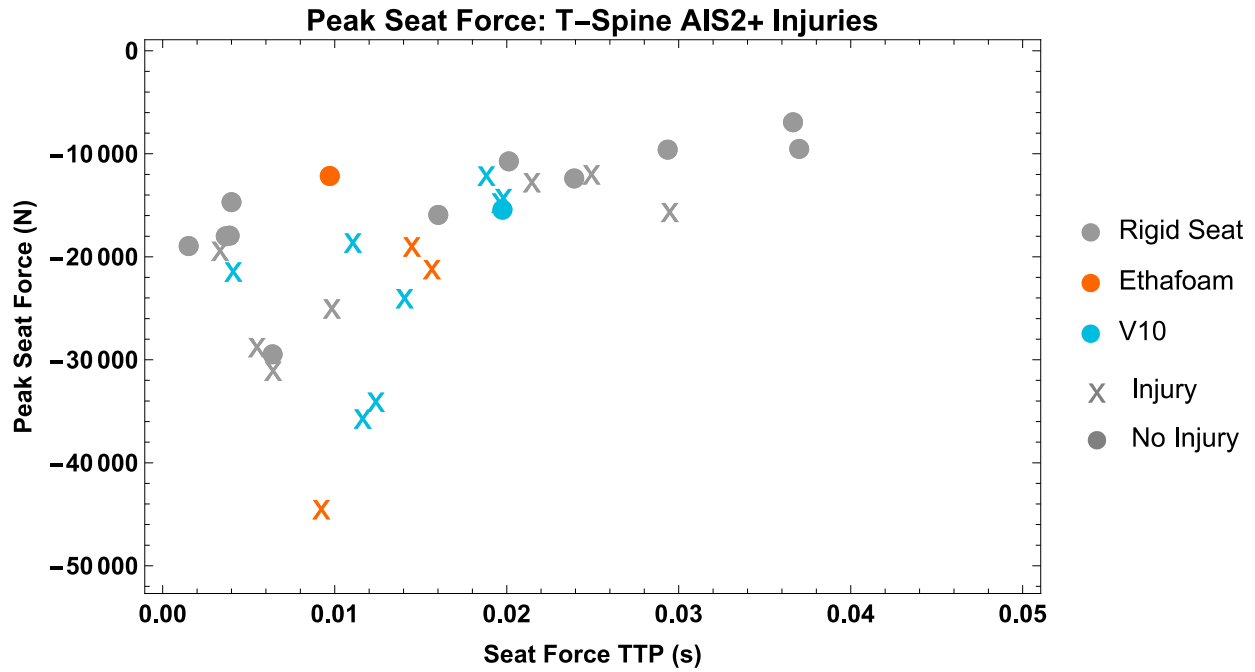


Figure 24. Effects of peak seat loads on AIS2+ thoracic spine injuries

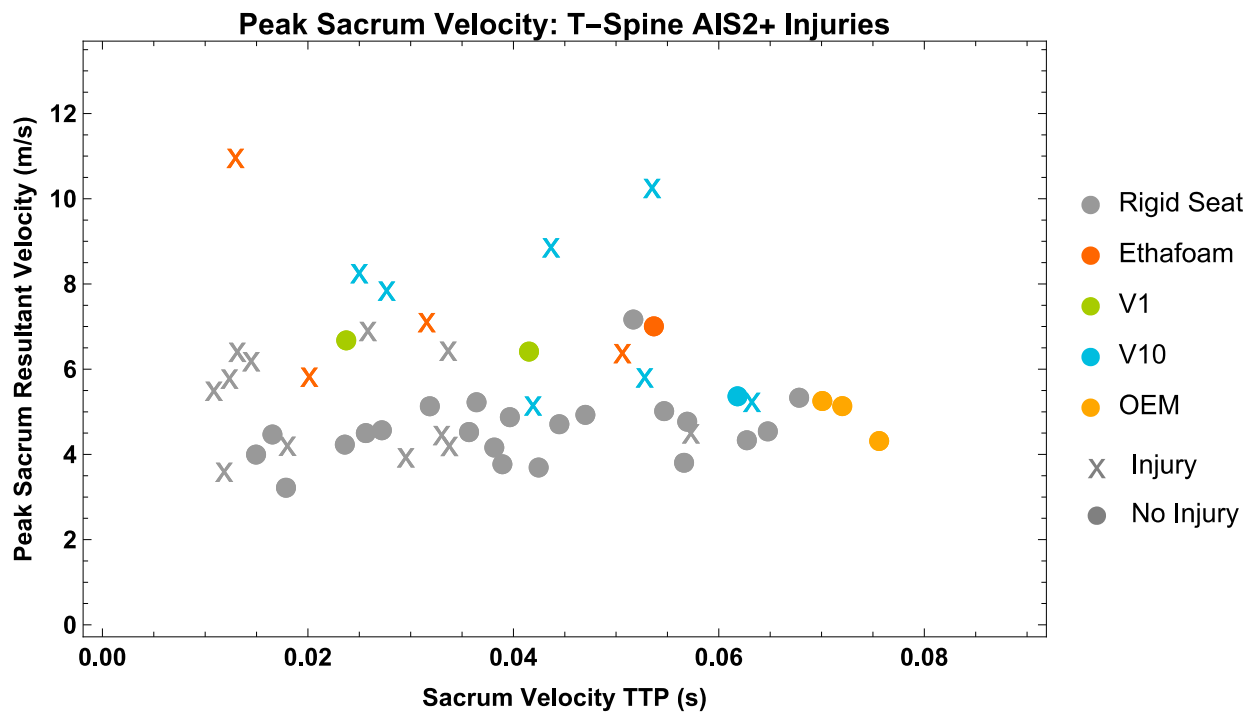


Figure 25. Effects of peak sacrum velocity on AIS2+ thoracic spine injuries

3.2 Relationship between Floor Loads and Pulse Duration on Foot and Ankle Injuries

To evaluate the occurrence of lower extremity injuries, a number of plots were generated to discern the effects of both magnitude and duration of loading on the lower extremity. The first of these is the peak force applied to the foot relative to the TTP of that force, as shown in Figure 26. In this plot, peak foot force represents the force applied to either foot (i.e., not across both feet) by the floor. As ancillary and BRC tests did not generate foot and ankle injuries, these data points are all shown in grey, while the severe test conditions are each defined by individual colors on the plot. A single injury on a lower extremity is denoted by an “X”, while multiple injuries on a single lower extremity (i.e., left, or right, not the sum of both limbs) are denoted by a triangle.

Figure 26 suggests that injuries do occur with greater frequency as peak foot force increases. Additionally, the tests with multiple injuries occur at the largest peak force. In Figure 27, the same tests are plotted against heel force. From these plots, there is a general trend that heel force peaks later than the force across the whole foot, and as expected, heel forces are lower than across the whole foot. However, the heel force does not appear to be a better, or worse, predictor of foot and ankle injuries.

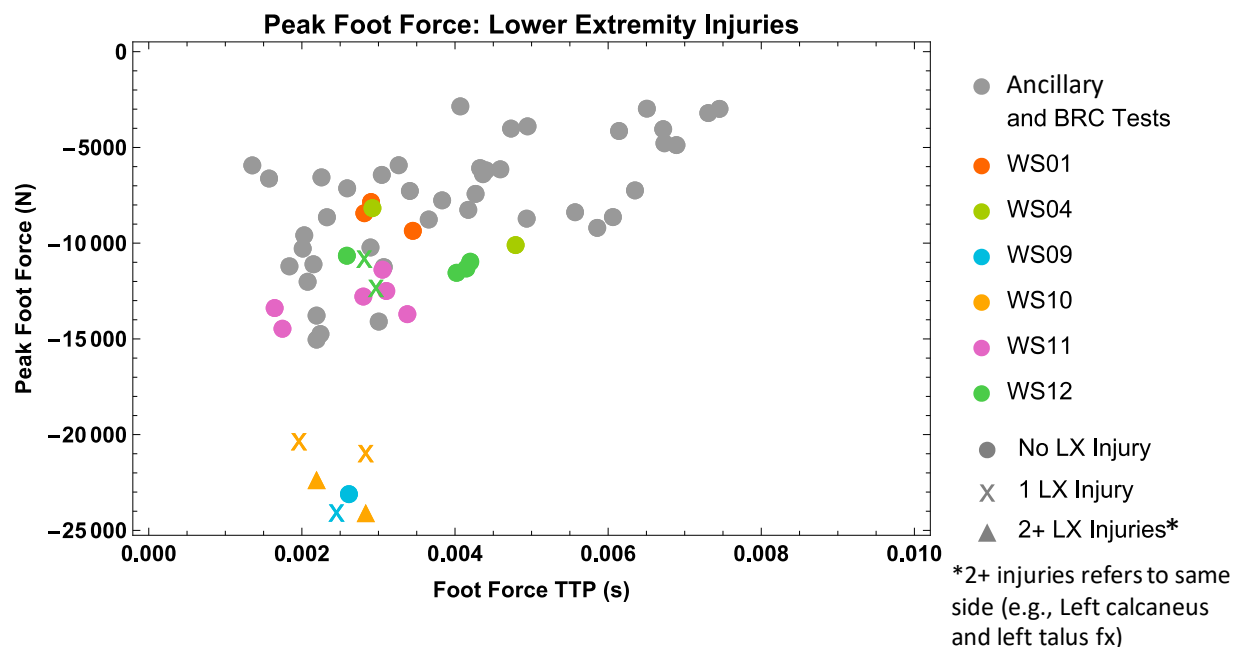


Figure 26. Effects of peak foot force and duration on lower extremity injuries

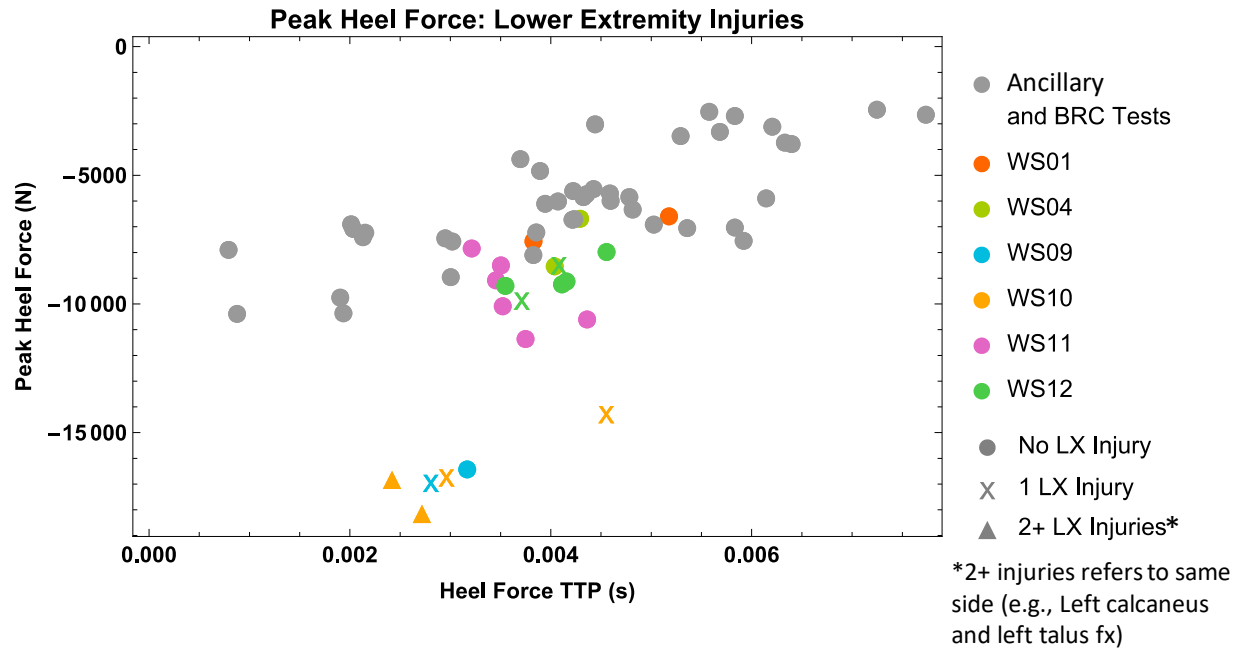


Figure 27. Effects of peak heel force and duration on lower extremity injuries

As a final alternative to foot load, total impulse and duration was evaluated for these lower extremity injuries, as shown in Figure 28. While injuries remain at greater magnitudes of impulse as a trend, there is no clear threshold, and duration does not appear to play a role for the range of data shown in the plot, which suggests that other factors play a strong role in the determination of injury.

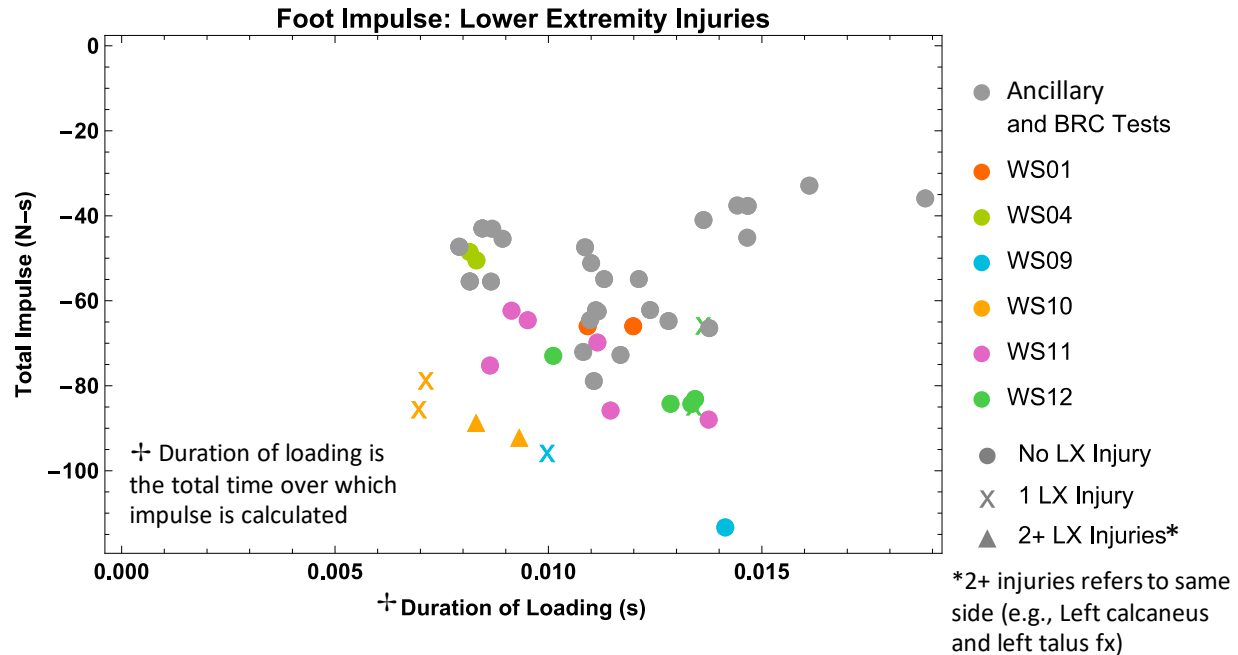


Figure 28. Effects of total foot impulse and duration on lower extremity injuries

3.3 Mechanism of Femur Fracture

From the 23 whole-body tests conducted at APL, there were only 2 tests that resulted in femur fractures (both of the right femur), WH04-002 and WS10-001. Both tests had different input conditions and seat pad configuration. However, both tests were conducted with PPE and had a relatively younger specimen with similar anthropometry. The specimens are listed in Table 26 and the test conditions are listed in Table 27. Both specimens were positioned based on specified requirements and fitted with similar instrumentation packages. The initial pretest position of both specimens is shown in Figure 29. Note that for WH04-002, the specimen had both right and left forearms removed prior to testing, while for WS10-001, only the left forearm was removed. Also, while the weights of both specimens were similar, it is clear from Figure 29 that weight distribution was different for both specimens, with more weight located in the legs of WH04-002 compared to the thin legs of WS10-001.

Table 26. WH04-002 and WS10-001 Specimen Information

BMI	Test ID	Specimen	Age (yrs)	Gender	Height (cm)	Weight (kg)	T-Score (L1-L4)
27.3	WH04-002	S150182	57	M	177.8	86.2	-0.8
26.0	WS10-001	16-10009	59	M	182.9	86.2	1.0

Table 27. WH04-002 and WS10-001 Test Conditions

Test ID	Floor Peak Velocity (m/s)	Floor TTP (ms)	Seat Peak Velocity (m/s)	Seat TTP (ms)	PPE	Posture	Seat Padding
WH04-002	6.0	3.9	4.0	9.5	Med	90 - 90 - 90	None
WS10-001	15.1	2.8	9.7	7.5	Med	90 - 90 - 90	V10

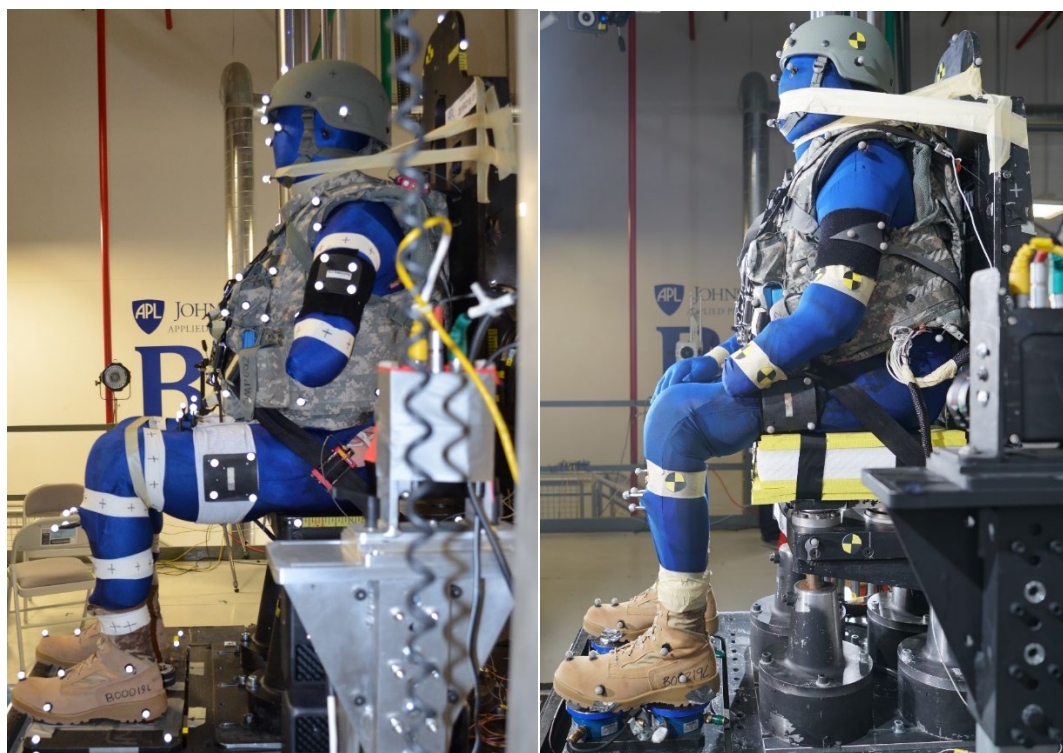


Figure 29. Initial positioning WH04-002 (left) and WS10-001 (right)

Posttest CTs and dissections documented the femur fractures for both specimens. For WH04-002, the fracture was characterized as a mildly displaced intertrochanteric fracture, while the fracture WS10-001 was classified as a displaced mid-shaft spiral wedge fracture. The fractures are documented in Figure 30. Note that prior to the transport of the WS10-001 specimen to the CT, the femoral fracture had not yet been detected, so specimen transport was noted as potentially having disturbed the fracture location, leading to further displacement. While both fractures occurred in anatomically different regions of the femur, both demonstrated spiral fracture patterns, suggesting a torsional failure mechanism.



Figure 30. Femoral fractures of WH04-002 (top) and WS10-001 (bottom)

Although these femoral fractures only occurred in 2 out of the 23 whole-body tests at APL, the relative severity of these fractures, as well as the uniqueness of these injuries, encouraged additional investigation. In Figure 31, vertical accelerations at the femurs for both WH04-002 and WS10-001 are plotted. As is seen in the figure, both fractures occur after the initial accelerative loading at the end of the acceleration, or at the peak vertical velocity. While WH04-002 fracture occurred at around 7 ms post loading, WS10-001 occurred around 12 ms.

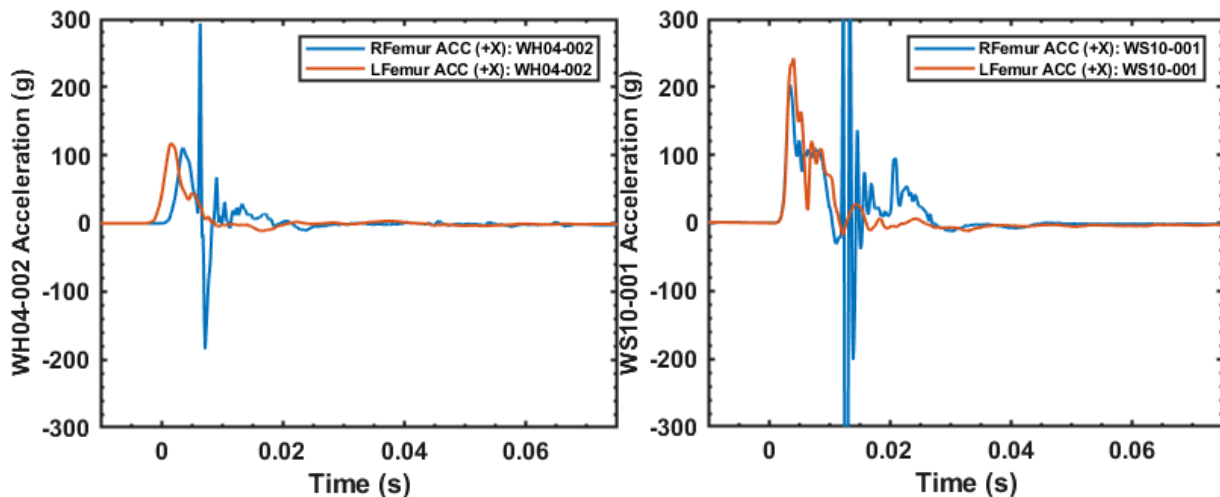


Figure 31. Vertical femoral acceleration of WH04-002 (left) and WS10-001 (right)

WH04-002 did not include load cell data, so we were only able to review response data from WS10-001. Looking at the seat force response data in Figure 32, the fracture timing appears to occur at the peak force response. Additionally, the peak force for the right thigh was higher than that of the left with a peak of approximately 7 kN. Note that this was the side of the specimen that also included a right forearm, as opposed to the left where the forearm was removed. Another test run at the same input condition (WH04-001), which had the right forearm removed and the left forearm intact, demonstrated a similar trend, where the peak thigh force was higher on the side with the intact forearm, as shown in Figure 33. Note that the peak thigh force was below the 7 kN seen in WS10-001, under which femur fracture was observed. While this may imply a correlation between peak thigh force and injury, it is expected that at least one other factor (probably several other factors) plays a role in these types of injury.

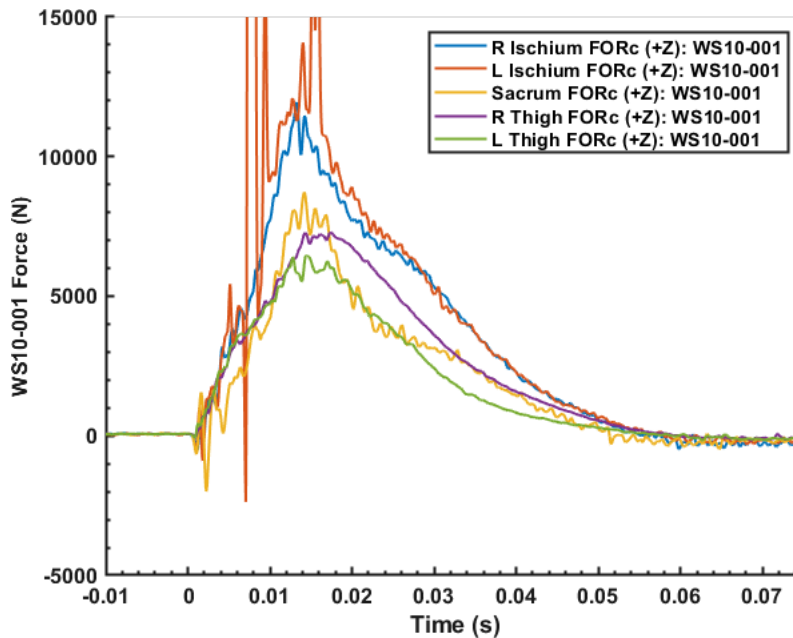


Figure 32. Seat force response for WS10-001; note the spikes in the signal are indicative of cable yank

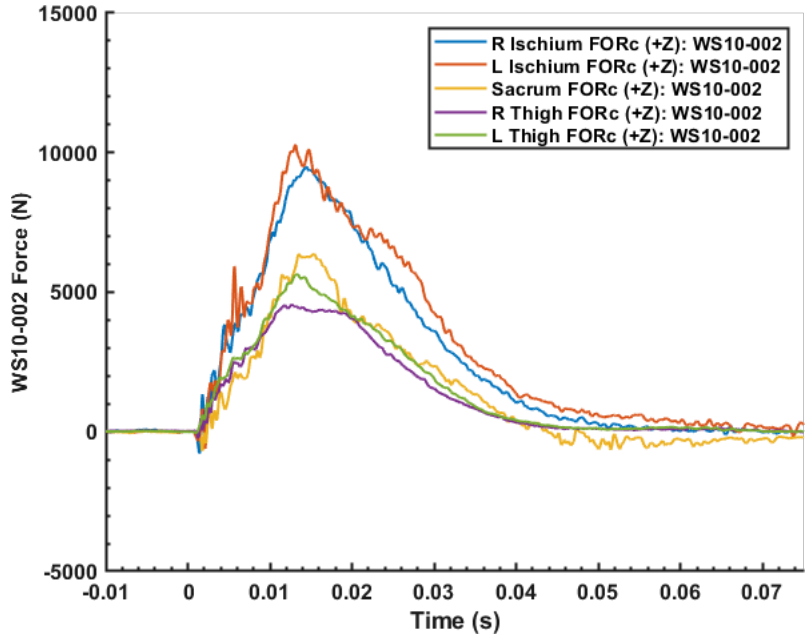


Figure 33. Seat force response for WS10-002

Another potential factor affecting the incidence of this type of injury is the presence of the medium IOTV. Note that the majority of tests that included the IOTV, conducted over a broad range of conditions, did not result in femoral fractures. Therefore, the presence of the IOTV is likely not the only factor leading to femoral fracture, but the IOTV may be a contributing factor. To investigate the interaction between the femur and the IOTV, femoral motion was tracked using high-speed video data for WH04-001 and WH04-002, which were both run under the same input conditions (Figure 34). From this figure, it is noted that the IOTV motion for WH04-002 initiates at about 7 ms, which corresponds to the timing of the femur fracture. This timing is demonstrated by the acceleration data shown in Figure 31 (at the left), where a high-frequency component of the response is observed. This implies that interaction between the femur and the IOTV may contribute to injury. However, further investigation is needed.

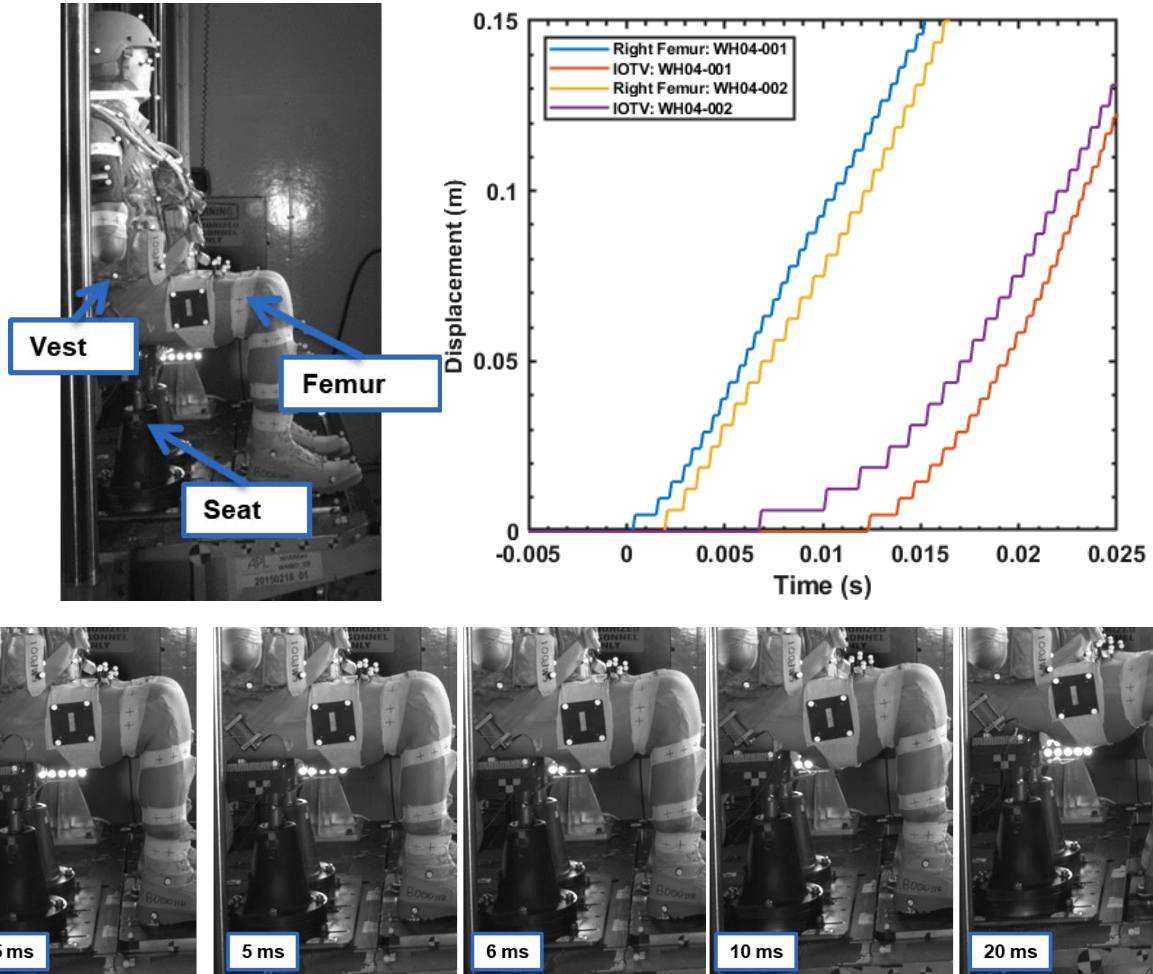


Figure 34. Kinematic displacement of WH04-001 and WH04-002 (top) and time-series images for WH04-002 (bottom)

In summary, out of the total number of whole-body tests at APL, only two specimens had femoral fractures. Both of these specimen were similar in height, weight, age, and bone mineral density, but were tested under substantially different input conditions. The resulting femur fractures were both on the right side, but were different in anatomical location, and both implied a twisting component to the fracture mechanism along with bending. From the load cell data in WS10-001, it appears that a force threshold of 7 kN is needed to induce this type of fracture. Further, from the WH04-002 kinematic tracking, the presence of the IOTV appears to potentially play some part in the incidence of fracture. Due to the limited number of specimens that had femoral fractures, as well as all the number of potential confounding variables, it is recommended that further study be done to investigate this injury mechanism.

4. DISCUSSION AND CONCLUSIONS

A range of injurious and noninjurious whole-body experiments have been completed in the WIAMan program to date. The injuries from these tests are summarized in Figure 35. The primary utility for the injury outcomes from these experiments is to serve as a data set to verify and validate injury prediction capabilities to be utilized in UBB experiments, which is an independent effort being conducted by the U.S. Army. That task will evaluate injury outcomes against ATD and other available data. Distribution, frequency, and severity of injuries from these experiments may be compared to Warfighter injuries reported in Danelson et al. (2018). It is intended that the utility of this data set will be far reaching and benefit Warfighter survivability in many ways.

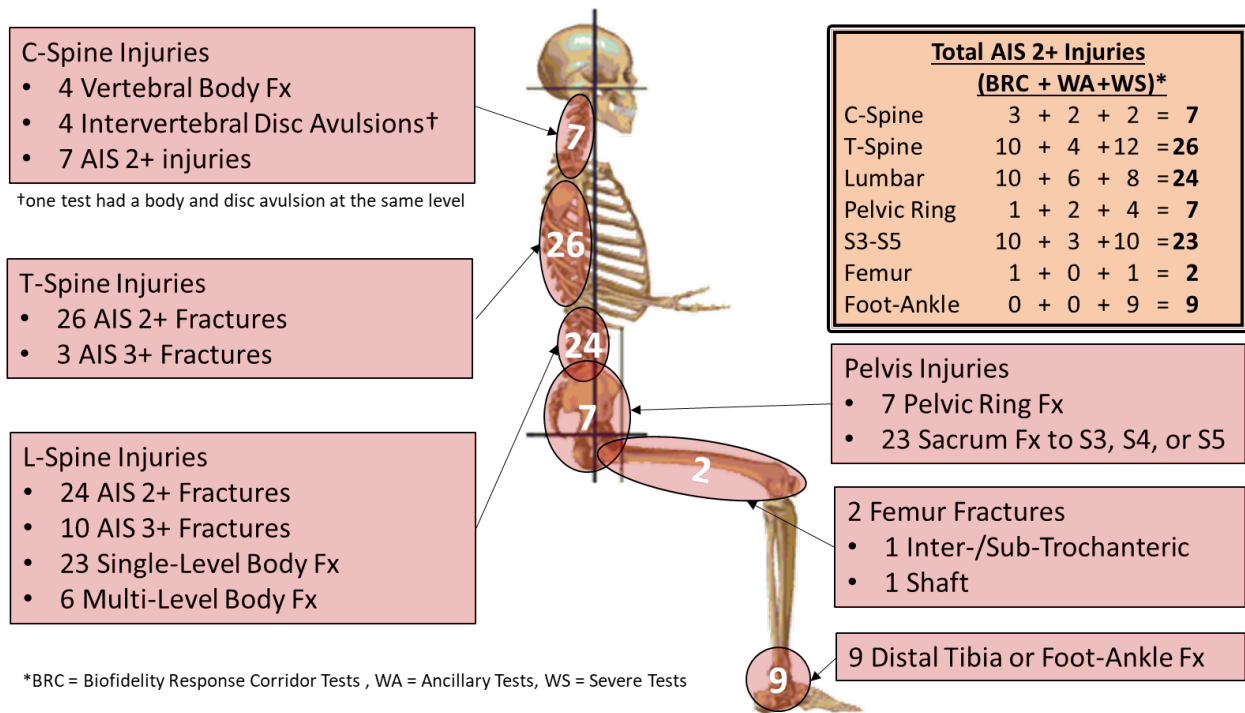


Figure 35. Total injuries from WIAMan whole-body experiments

Analyses conducted in this report have focused on the most direct outcomes of seat loading as well as floor loading. Based on seat loading, disruption of the pelvic ring was observed with increased seat loads. Sacral fractures were observed at lower seat loads, especially with a rigid seat. Although, sacral fractures remain likely with increased seat loads across seating conditions. Data suggest a threshold seat loading value for these injuries, but the cutoff is not clear and more investigation is needed.

Lumbar fractures were observed to occur throughout the distribution of tests that were evaluated when AIS2+ injuries were considered. However, data suggest an increased seat loading threshold for AIS3+ injuries. It is unclear whether TTP has a strong influence on lumbar injury, because shorter TTPs were associated with increased seat forces in these tests. This association between high-magnitude and short-duration loading may result from the selection of UBB-relevant input conditions. Similar trends were seen for thoracic injuries. While the rigid seat condition did tend to produce increased sacral fractures, these effects were less evident for other spinal injuries.

Seat loads were observed to be a better metric of injury than sacrum velocity. While this may be due to the strong relationship between load and fracture, sacrum velocity may not be the ideal metric due to the location at which velocity is measured. More work is needed to consider velocity taken about a different location that may be less sensitive to pelvic rotations and other perturbations to these measurements.

Foot and ankle data that were presented suggest that loads applied across the heel, or across the whole foot, demonstrate similar trends relative to foot and ankle injury. Impulse showed some correlation, although not as clear as load. However, a limited number of foot and ankle injuries were available for evaluation in this study. More work is needed to evaluate foot and ankle injuries in the whole body.

5. REFERENCES AND DOCUMENTS

- Bass, C. R., Danelson, K., Agnew, A., Gayzik, F. S., Rupp, J. D., Stitzel, J., Yoganandan, N., & Voo, L. (2013). *W0080: minimum pre-test anthropometry requirements for scaling*.
- Bass, C. R., Agnew, A., Gayzik, F. S., Rupp, J. D., Stitzel, J., Yoganandan, N., Marcus, I., & Voo, L. (2016). *W0084: PMHS scaling methods for biofidelity response corridors*.
- Danelson, K., Watkins, L., Hendricks, J., Frounfelker, P., WIAMan Case Review Team, Pizzolato-Heine, K., Valentine, R., & Loftis, K. (2018). Analysis of the frequency and mechanism of injury to warfighters in the under-body blast environment. *Stapp Car Crash J.* 62, 489–513.
- Gayzik, F. S., Pintar, F. A., Baker, A. Bass, C. R., Bannerjee, A., et al. (2017). *W0063: guidance document for HIPC development*.
- Reed, M. P. & Ebert, S. M. (2013). *The seated soldier study: posture and body shape in vehicle seats*. University of Michigan Transportation Research Institute (UMTRI).
<http://www.umtri.umich.edu/our-results/publications/seated-soldier-study-posture-and-body-shape-vehicle-seats>.
- Rupp, J. D., Miller, C., Zaseck, L. W., Orton, N., Bonifas, A., Slykhouse, L., & Reed, M. P. (2016). Forces applied to the foot and pelvis in high rate vertical accelerative loading. In *Proceedings of the 2016 Summer Biomechanics, Bioengineering, and Biotransport Conference* (No. 2016-896).
- Rupp, J. R. & Reed, M. P. (2015). *Draft PMHS positioning procedures 9/Dec/2015. Version 0.7*.
- Slykhouse, L., Zaseck, L. W., Miller, C., Humm, J.R., Alai, A., Kang, Y. S., Dooley, C., Sherman, D., Bigler, B., Demetropoulos, C. K., Reed, M. P., Rupp, J. D. (2019 July). Anatomically-based skeletal coordinate systems for use with impact biomechanics data intended for anthropomorphic test device development. *J Biomech.* 19(92), 162–168.
- Spink, R. (2014, September). *A simple method for processing measurements of vehicle response to underbody blast during live fire test and evaluation*. (Report No. ARL-TR-7030). U.S. Army Research Laboratory.
- WIAMan Biomechanics Team. (2013a, September). *W0058: Warrior Injury Assessment Manikin (WIAMan) Project Helmet Fitting Procedures*. Version 1.1 [unpublished].
- WIAMan Biomechanics Team. (2013b, September). *W0059: Warrior Injury Assessment Manikin (WIAMan) Project Vest Fitting Procedures*. Version 1.1 [unpublished].
- WIAMan Biomechanics Team. (2013c, September). *W0060: Warrior Injury Assessment Manikin (WIAMan) Project Boot Fitting Procedures*. Version 1.0 [unpublished].
- WIAMan Biomechanics Team. (2013d, October). *W0070: Warrior Injury Assessment Manikin (WIAMan) Project Belt Fitting Procedures*. Version 1.1 [unpublished].

Appendix A – List of Acronyms

3-D	three-dimensional
6DOF	six-degree-of-freedom
ACH	advanced combat helmet
AIS	Abbreviated Injury Scale
ASIS	anterior superior iliac spine
ATD	anthropomorphic test device
BRC	biofidelity response corridor
CG	center of gravity
CT	computed tomography
HIPC	human injury probability curve
IARC	injury assessment reference curve
IOTV	improved outer tactical vest
JHU APL	The Johns Hopkins University Applied Physics Laboratory
L	lumbar
PMHS	postmortem human subject
PPE	personal protective equipment
PSIS	posterior superior iliac spine
SCoTT	Signal Conversion Tiger Team
T	thoracic
TTP	time to peak
UBB	under-body blast
UMTRI	University of Michigan Transportation Research Institute
VALTS	Vertically Accelerated Load Transfer System

WIAMan

Warrior Injury Assessment Manikin

WSU

Wayne State University

Appendix B – Glossary

Anthropomorphic test device (ATD): A physical device with size, shape, and biomechanical response characteristics representative of a target population of living humans. Embedded sensors within the ATDs enable the measurement of biomechanical responses associated with injury metrics-based IARCs. The correlation of these metrics to specific injuries enables the ATD to predict the probability of specific injuries in test and evaluation applications.

Biometric: Term for body measurements and calculations. In this report, it is used to refer to measurements of the lumbar spine response under the applied loading conditions.

Human injury probability curve (HIPC): A statistical relationship between the probability of a particular injury to a human and a continuous biometric directly measured or calculated from the measurements from physical tests of a PMHS.

Injury assessment reference curve (IARC): A mathematical relationship between the probability of a particular injury to a human and a continuous biomechanical parameter measured in physical tests or simulations (or calculated from the results of physical tests) using an ATD. The measurement locations for biometric of interest could differ between the ones captured in ATD tests for IARCs versus PMHS tests for HIPCs.

Injury metric: A biomechanical response quantity measured or derived from PMHS testing that has a statistical correlation to injury outcome and severity for a given bone or anatomical component (e.g., force, moment, acceleration, or strain). When multiple relevant metrics are available, statistical methods are used to determine the best predictor of PMHS injury (Gayzik et al., 2017).

Match-paired: A matching pair of a PMHS test and an ATD test based on their anatomical representation, inertial properties, and test conditions.

Personal protective equipment (PPE): A term for equipment worn for protection from a range of threats that may include helmets, body armor, and other materials.

Postmortem human subject (PMHS): A term for human cadaveric subjects serving as human surrogates in biomechanical tests that are partially representative of living human subjects of the target population.

Subject ID: A de-identified tracking number assigned by the tissue vendor to the subject.

Strength of design: A test designed to prove out the capability of a device or fixture at or near the expected limits of device survivability.

Test ID: An internal tracking number assigned to the subject within the organization where it is being tracked and tested.

Time to peak (TTP): The time from the start of a measured or calculated response until the signal reaches its peak. Calculated using the method defined in ARL-TR-7030 (Spink, 2014).

Warrior Injury Assessment Manikin (WIAMan): Army-sponsored program to develop an ATD specifically designed to predict injury risk in vertical loading environments.

Appendix C – Classification of Injuries

C.1. APPLIED PHYSICS LABORTORY INJURY CLASSIFICATION

Table C.1. APL Injury Summary

Test Series ID	Specimen ID	Description	AIS 2015	AIS 2015 Localizer(s)
WH01-002	BRC13011299	NO INJURIES		
WH01-003	BRC13011317	NO INJURIES		
WH01-004	BRC13122239	Left L4 TP fx	650620.1	2023
		Right L5 TP fx	650620.1	1024
WH03-001	BRC12121219	Bilateral L4 TP fx	650617.2	5823
		L2 left TP fx	650620.1	2021
		L4 VB fx (minor compression)	650632.2	0023
WH03-002	S142237	T6 Minor compression fx	650432.2	0013
		Right 6th anterior rib fx	450201.1	1036
WH03-003	15-09060	L2 bilateral TP fx	650617.2	5821
WH04-001	L141473	NO INJURIES		
WH04-002	S150182	L3 bilateral TP fx	650617.2	5822
		L4 bilateral TP fx	650617.2	5823
		L5 bilateral TP fx	650617.2	5824
		Sacrum fx with bilateral SI joint involvement	856161.3	50NN 00NR
		Coccyx fx	856151.2	00NW
		Intertrochanteric fx of right femur	853151.3	1000
WH04-003	S150678	NO INJURIES		
WH08-001	15-12028	L3 anterior body fx	650632.2	0122
		S3/S4 fx; coccyx laxity	856151.2	00NR
WH08-002	15-10034	Coccyx laxity		
WH08-003	15-00441	T5 endplate fx	650432.2	0012
		Coccyx fx	856151.2	00NW
		Lateral Right Rib 8 fx	450201.1	1038
WH12-001	S161437	Anterior Left Rib 3-6 fx	450203.3	2133 2134 2135 2136
WH12-002	16-04013	NO INJURIES		
WH12-003	S161490	NO INJURIES		
WS10-001	16-10009	Left calcaneus fx - unstable	857371.2	2000
WS10-001	16-10009	T11 anterior body fx (minor)	650432.2	0018
		T12 right tp fx	650420.1	1000
		L1 VB fx, minor ht loss	650632.2	0020
		L2 bilateral TP fx	650617.2	5821
		L4 spinous process fx	650618.2	0023

Test Series ID	Specimen ID	Description	AIS 2015	AIS 2015 Localizer(s)
		L5 burst fx, major ht loss	650634.3	0024
		Right rib 3,6,7,9,10 postero-lateral fx	450203.3	3433 3436 3437 3438 3439 3440
		Left ribs 2,4,5,10,11 postero-lateral fx	450203.3	4432 4434 4435 4440 4441
		Bilateral fx of S1-S5 consistent with vertical shear fx to acetabulum (complete disruption)	856171.4	00NW 00NR 20NN 10NN
		Right femur fx	857271.3	1000
		Right calcaneus fx - unstable	857371.2	1000
		Left talus fracture	857251.2	2000
		Right talus fracture	857251.2	1000
WS10-002	1612325R	C4 anterior body fx	650232.2	0004
		C6 spinous process fx	650218.1	0006
		T1 spinous process fx	650618.1	0008
		T8 anterior body fx	650432.2	0015
		L1 right tp fx and spinous process fx	650617.2	1820 9520
		L2 left tp fx	650620.1	2821
		L3 vb fx major ht loss (burst)	650634.3	0022
		L4 spinous process fx	650618.2	0023
		L5 bilateral tp fx, spinous process fx	650617.2	5824 9524
		Bilateral rib 1-12 postero-lateral fx	450203.3	5331 5332 5334 5335 5336 5337 5338 5339 5340 5341 5342
		Bilateral sacrum fx at S3, stable	856151.2	00NR
		L calcaneus fx	857371.2	2000
		R talus fx	857261.2	1000
WS10-003	F182258	T12 superior body fx	650432.2	0019
WS10-003	F182258	L1 right tp fx	650620.1	0020
		L2 anterior body fx, minor ht loss	650632.2	0021
		L2/L3 disc disruption	650699.2	0021
		L5 anterior body fx (minor height loss) and TP fx	650617.2	0024
		Right ribs 2-5 fx	450203.3	1032 1033 1034 1035
		Left ribs 5-6 fx	450203.3	2035 2036

Test Series ID	Specimen ID	Description	AIS 2015	AIS 2015 Localizer(s)
		Pelvic ring fx: complete disruption (left superior pubic ramus, pubic symphysis, bilateral fx of S1-S5)	856171.4	24NV 00NS 00NR
		Rt Cuneiform fx	857551.2	1000
		Rt Metatarsal fx	857173.2	1000
		Rt Pilon fx	854371.2	1000
		Rt Fibula fx	854461.2	1000
		Lt Calcaneus fx	857371.1	2000
		Rt Calcaneus fx	857371.1	1000
		Lt talus fx	857251.2	2000
		Lt cuboid fx	857600.2	2000
		Lt cuneiform fx	857551.2	2000
		Lt metatarsal fx 3-5	857173.2	2000
WS04-001	S170374	T7 anterior wedge fx	650432.2	0014
		T8 anterior wedge/endplate fx	650432.2	0015
		L1 anterior body fx	650632.2	0020
		L2 wedge fx	650632.2	0021
		L3 wedge/endplate/posterior arch fx	650636.3	0022
		Sacrum fx	856151.2	00NR
WA01-001	586A00988	C5 VB fx - minor compression	650232.2	0005
WA04-001	6673	T12 compression fx - major compression	650434.3	0019
		L4 left TP fx	650620.1	2023
		L5 left TP fx	650620.1	2024
WA04-001	6673	Pelvic ring fx: right ilium, bilateral SI joint fx, left sacrum fx	856171.4	10NT 50NN 20NR
WA06-001	S151345	C6 VB fx - minor compression	650232.2	0006
		T4 VB fx - minor compression	650432.2	0011
		T5 left TP fx	650420.1	2012
		L1 bilateral TP fx	650617.2	5820
		L2 bilateral TP fx	650617.2	5821
		L3 VB fx - major compression	650634.3	0022
		Left rib 2-4 posterior fx, Right rib 12 posterior fx	450203.3	2332 2333 2334 1342
WA07-001	S151697	T8 vertebral body softening		
		L4 left TP fx	650620.1	2023
		L5 compression fracture with pedicle fracture - burst	650636.3	0024

Test Series ID	Specimen ID	Description	AIS 2015	AIS 2015 Localizer(s)
		Right lateral rib 8 fracture, Left lateral rib 7 fracture	450202.2	3238 4237

C.2. WAYNE STATE UNIVERSITY INJURY CLASSIFICATION

Table C.2. WSU Injury Summary

Test Series ID	Specimen ID	Description	AIS 2015	AIS 2015 Localizer(s)
WH01-001	OSU6725	Right odontoid fx	650228.3	1001
		C1-C2 subluxation	650206.3	0001
		T11 superior endplate fx	650416.2	0018
		T12 compression fx	650432.2	0019
		Transverse sacrum fx at S4	856151.2	00NR
WA03-001	BRC13122202	T11 compression fx	650432.2	0018
		L1 transverse process fx	650620.1	0020
		L2 transverse process fx	650620.1	0021
		L3 transverse process fx	650620.1	0022
		L4 transverse process fx	650620.1	0023
		L5 transverse process fx	650620.1	0024
		Right rib 11 fx	450203.3	1041
		Right acetabulum fx	856251.2	10NQ
WH03-001	OSU6908	Pelvic ring fx	856171.4	00NR
		L1 impaction fracture	650630.2	0020
WH03-002	LMD14-0355	L3 compression fx (minor)	650632.2	0022
WH04-001	S150758	Separation of disc between T12-L1	650499.2	0019
		T12 VB fx at mount location	650430.2	0019
		Right rib 1-4, 7, left rib 2-3 Fx	450213.4	1031, 1032, 1033, 1034, 1037, 2032, 2033
		Sternum fx	450804.2	0070
WH04-002	S151176	Transverse anterior fx at S5 and Co1	856151.2	00NR 00NW
WH04-003	S151317	L2 left transverse process fx	650620.1	2021
WH06-001	LL15-10028	C5/C6 fx (avulsion of disc from inferior endplate of C5 and superior endplate of C6)	650230.2	0005

Test Series ID	Specimen ID	Description	AIS 2015	AIS 2015 Localizer(s)
		L1 compression fx at superior endplate	650632.2	0020
WH06-002	LL16-01011	NO INJURIES		
WH06-003	LL16-02045	C5/C6 avulsion fx	650230.2	0005
WS11-001	L171491	T4 minor compression VB fx	650432.2	0011
		T5 VB fx, minor compression	650432.2	0012
		T10 minor compression VB fx	650432.2	0017
		Pelvic ring fx: stable (S4-S5)	856151.2	00NR
WS11-002	S172105	T5 compression fx (minor)	650432.2	0012
		T6 compression fx (minor)	650432.2	0013
WS11-003	S160979	T4 minor compression fx	650432.2	0011
		T5 minor compression fx	650432.2	0012
		T7 minor compression fx	650432.2	0014
		T8 minor compression fx	650432.2	0015
		L2 bilateral TP fx	650617.2	5821
		L4 bilateral TP fx	650617.2	5823
		L5 bilateral TP fx	650617.2	5824
		L5 compression fx (major)	650634.3	0012
WS09-001	S160712	C4-C5 disk avulsion	650200.2	0004
		Compression fx at T7 (major)	650436.3	0014
		Compression fx at T8	650432.2	0015
		L5 comminuted spinous process fx	650618.1	0024
		Sacrum fx at S3	856151.2	00NR
		Sternum fx	450804.2	0000
		Pelvic ring fx, unstable	856171.4	10NN 20NN 00NS 15NV 25NV 24NV 00NR
		Right calcaneus fx	857371.1	1000

C.3. UNIVERSITY OF MICHIGAN TRANSPORTATION RESEARCH INSTITUTE INJURY CLASSIFICATION

Table C.3. UMTRI Injury Summary

Test Series ID	Specimen ID	Description	AIS 2015	AIS 2015 Localizer(s)
WH01-001	6600	L4 VB fx w/o ht loss; anterior superior endplate	650632.2	0023
		T5 left lamina fx	650424.2	2012
		Rib fx: right ribs 6, 7, 8	450203.3	1036 1037 1038
WH02-001	6899	L3 right transverse process fx	650620.1	1022
		S3 fx	856151.2	00NR
		Coccyx fx (bilateral)	856151.2	00NW
WH02-002	6944	S5 fx	856151.2	05NR
WH02-003	14-00364	L3 superior endplate depression 3-4mm	650632.2	0022
		L4 VB fx w/ 8-9 mm depression	650632.2	0023
WH02-004	S150268	S4 fx	856151.2	05NR
WH7-001	15-12011	T12 fracture - extending through inferior and superior endplates; anterior	650417.2	0419 0519
		S4/Coccyx fx - pelvic ring STABLE	856151.2	05NR 00NW
WH7-002	35064	L1 spinous process fx	650618.1	0020
		L2 vb fx involving posterior elements (right pedicle)	650617.2	9021 1721
		S4 / coccyx fx	856151.2	05NR 00NW
WH7-003	16-01020	T7 VB fx - <20% ht loss, inferior endplate involved	650432.2	0014
		S5 fx	856151.2	05NR
WH11-001	S161495	T12 VB fx; anterior wedging	650432.2	0019
		Coccyx fx	856151.2	00NW
WH11-002	16-07027	T6 superior endplate fx; no ht loss	650432.2	0013
		L2 vb fx; anterior superior; no ht loss	650632.2	0021
WH11-003	16-08019	T7 VB fx; no ht loss	650432.2	0014
		T11 VB fx; no ht loss (anterior-superior)	650432.2	0018
WH11-003	16-08019	L1 VB fx; no ht loss; anterior-superior endplate	650632.2	0020
WA05-001	15-00396	T5 spinous process fx	650418.1	0012
		T6 spinous process fx	650418.1	0013

Test Series ID	Specimen ID	Description	AIS 2015	AIS 2015 Localizer(s)
		T7 spinous process fx	650418.1	0014
		Right L1 TP fx	650620.1	1020
		L3 VB fx (burst)	650636.3	0022
		proximal coccyx fx	856151.2	00NW
WA08-001	15-08052	Bilateral T11 tp fx	650417.2	5818
		Right T10 tp fx	650420.1	1017
		rupture of T12/L1 supraspinous ligament	640484.1	0019
		L1 burst fx	650636.3	0020
		Bilateral L1 tp fx	650617.2	5820
		Right L2 tp fx	650620.1	2021
		Left Rib 12 fx at costovertebral articulation	450201.1	2042
WA09-001	34910	T5 spinous process fx	650418.1	0012
		L1 VB fx with ht loss	650632.2	0020
		L4 vb fx w/ ht loss	650632.2	0023
		Grade 1 anterolisthesis of L5 on S1	650604.2	0024
		S5 fx	856151.2	00NR
		Right anterior rib fx (ribs 1,2,3,5,6) and left anterior rib fx (ribs 3,4) anterior angulated right rib fx (rib 4)	450209.3	1131 1132 1133 1134 1135 1136 2133 2134
WA02-001	6858	T7 VB fx, minor compression	650432.2	0014
		L1 bilateral TP fx	650617.2	5820
		L2 bilateral TP fx	650617.2	5821
		L3 left TP fx	650620.1	2022
		L4 bilateral TP fx, VB fx with >20% ht loss *Possibly caused by instrumentation	650636.3	0023
		Sacrum fx (S3-S5, bilateral), coccyx fx @ Co1, Co3	856151.2	00NR 00NW
		Ruptured supraspinous ligament	640484.1	0000
		Fractured manubrium	450804.2	0400
		Dislocated medial end of right clavicle	770530.2	1000
		Fractured ribs: Left: 2, 7, 8; Right: 1, 2, 12	450203.3	1031 1032 1042 2032 2037 2038
WS01-001	S161876	T7 anterior wedging fracture	650432.2	0014
		T12 superior endplate fracture	650432.2	0019
		L2 inferior endplate fracture	650632.2	0021
		L3 superior endplate fracture	650632.2	0022

Test Series ID	Specimen ID	Description	AIS 2015	AIS 2015 Localizer(s)
		Coccyx fracture	856151.2	00NW
WS01-002	35286	T9 superior endplate fracture	650432.2	0016
		L2 burst fracture	650636.3	0021
		Sacrum fracture at S5	856151.2	00NR
WS12-001	35249	Spinous process fx at T6	650418.1	0013
		Pelvic ring fx; bilateral posterior instability	856171.4	00NR 10NN 20NN
WS12-002	L162663	T12 lamina and posterior body fx (instrumentation a factor)	650417.2	0619 9019
		L1 vb fx - major compression	650634.3	0020
		Bilateral S4/S5 fx	856151.2	00NR
		Rt calcaneus fx	857371.2	1000
WS12-003	L170249	T4 lamina and body fx (pre-existing T4 fusion to T3)	650417.2	0611 9011
		T12 vb fx (burst)	650436.3	0019
		L1 bilateral TP fx	650617.2	5820
		L4 bilateral TP fx	650617.2	5823
		L5 bilateral TP fx	650617.2	5824
WS12-003	L170249	Pelvic ring fx: complete disruption; Left and right iliac wing, right superior and inferior ramus, right ischial tuberosity, right and left ischial spine fx, severe sacrum fx at and below S3	856171.4	10NT 20NT 00NW 10NV 10NU 00NR
		Left calcaneus fx	857371.2	2000

Appendix D – Distribution List

ORGANIZATION

U.S. Army CCDC Data & Analysis Center
FCDD-DAS-LBW
K. Loftis
D. Barnes
Aberdeen Proving Ground, MD 21005

U.S. Army CCDC Army Research Laboratory
FCDD-RLD-CL/Tech Library
2800 Powder Mill Rd.
Adelphi, MD 20783-1138

Defense Technical Information Center
ATTN: DTIC-O
8725 John J. Kingman Rd.
Fort Belvoir, VA 22060-6218